

## Satellite-based assessment reveals hydrological and ecological transformations from China's South-to-North Water Diversion Project

Aoxue Cui, Chao Wang, Shuzhe Huang, Renke Ji, Mingming Jia, Xiang Zhang, Wei Wang & Nengcheng Chen

**To cite this article:** Aoxue Cui, Chao Wang, Shuzhe Huang, Renke Ji, Mingming Jia, Xiang Zhang, Wei Wang & Nengcheng Chen (03 Sep 2025): Satellite-based assessment reveals hydrological and ecological transformations from China's South-to-North Water Diversion Project, *Geo-spatial Information Science*, DOI: [10.1080/10095020.2025.2541071](https://doi.org/10.1080/10095020.2025.2541071)

**To link to this article:** <https://doi.org/10.1080/10095020.2025.2541071>



© 2025 Wuhan University. Published by Informa UK Limited, trading as Taylor & Francis Group.



[View supplementary material](#)



Published online: 03 Sep 2025.



[Submit your article to this journal](#)



Article views: 536



[View related articles](#)



[View Crossmark data](#)



Citing articles: 1 [View citing articles](#)

# Satellite-based assessment reveals hydrological and ecological transformations from China's South-to-North Water Diversion Project

Aoxue Cui <sup>a</sup>, Chao Wang <sup>a,b,c</sup>, Shuzhe Huang <sup>a</sup>, Renke Ji <sup>a</sup>, Mingming Jia <sup>d</sup>, Xiang Zhang <sup>b</sup>, Wei Wang <sup>a</sup> and Nengcheng Chen <sup>b</sup>

<sup>a</sup>State Key Laboratory of Information Engineering in Surveying, Mapping and Remote Sensing, Wuhan University, Wuhan, China; <sup>b</sup>National Engineering Research Center of Geographic Information System, School of Geography and Information Engineering, China University of Geosciences (Wuhan), Wuhan, China; <sup>c</sup>Key Laboratory of Basin Water Resources and Eco-Environmental Science in Hubei Province, Changjiang River Scientific Research Institute of Changjiang Water Resources Commission, Wuhan, China; <sup>d</sup>State Key Laboratory Black Soils Conservat & Utilizat, Northeast Institute of Geography and Agroecology, Chinese Academy of Sciences, Changchun, China

## ABSTRACT

The Middle Route of the South-to-North Water Diversion Project (MR-SNWDP) in China, as the largest inter-basin water transfer initiative in the world, has profoundly influenced the regional hydrology, ecology and climate of both the Water Source Areas (WSA) and Water Receiving Areas (WRA). This study aimed to comprehensively assess the long-term environmental impacts of the MR-SNWDP from 2004 to 2023, with particular emphasis on vegetation dynamics in response to both climatic and anthropogenic drivers. It addressed a critical knowledge gap regarding the spatially heterogeneous ecosystem responses to large-scale hydrological interventions under climate variability. Utilizing satellite-derived datasets including GRACE Terrestrial Water Storage Anomalies (TWSA) for hydrological variations and MODIS Normalized Difference Vegetation Index (NDVI) for vegetation activity, we combined trend analysis with attribution modeling to explore the spatiotemporal patterns of environmental change. The findings highlighted that the MR-SNWDP has significantly alleviated water shortages in the WRA by increasing surface water storage and reducing groundwater extraction. This shift in water accessibility promoted vegetation growth, particularly in cropland regions, by extending the growing season through earlier greening and delayed senescence. Climatic factors such as precipitation and temperature were the dominant positive drivers of NDVI, while anthropogenic stressors, including urban expansion and agricultural intensification, exerted negative effects. However, the influence of climatic factors on vegetation dynamics weakened in the WRA following the project's implementation, while the impacts of human activities became more prominent. This trend was attributed to the long-term redistribution of water resources under the MR-SNWDP, which mitigated water scarcity and rendered vegetation growth less sensitive to climatic fluctuations. Furthermore, vegetation recovery contributed to regulating urban microclimate and mitigating the urban heat island effect, reflecting broader ecological benefits in the WRA. In contrast, the WSA experienced reduced vegetation activity and increased ecological vulnerability, emphasizing the need to balance inter-basin water transfers with local ecosystem sustainability.

## ARTICLE HISTORY

Received 23 February 2025  
Accepted 24 July 2025

## KEYWORDS

The Middle Route of the South-to-North Water Diversion Project (MR-SNWDP); hydrological and ecological impacts; remote sensing; water source and receiving areas

## 1. Introduction

Water is a fundamental resource for sustaining life and supporting socio-economic development on Earth (Gleick 2003). However, global water resources exhibit an uneven spatial and temporal distribution. This disparity has been further exacerbated by rapid urbanization, population growth, economic expansion and the intensifying impacts of climate change (Cosgrove and Loucks 2015; Jackson et al. 2001). According to the United Nations, approximately 70% of the global population lives in regions with insufficient annual precipitation, with over 3 billion people facing challenges in accessing clean water (Boretti and Rosa 2019;

Mekonnen and Hoekstra 2016). The overextraction of groundwater and unsustainable allocation of surface water have resulted in widespread river depletion, wetland degradation and biodiversity loss, amplifying ecological vulnerabilities worldwide (Scanlon et al. 2017; Vörösmarty et al. 2010). In China, the spatial imbalance between water availability and socio-economic demand is particularly severe. The southern regions with abundant precipitation hold over 70% of the total water resources. In contrast, the northern regions, which host 40% of the population and 60% of the arable land, receive less than 30% of the available water (Fan et al. 2015; Jiang 2009; Piao et al. 2010;

**CONTACT** Chao Wang  c.wang@whu.edu.cn

 Supplemental data for this article can be accessed online at <https://doi.org/10.1080/10095020.2025.2541071>

© 2025 Wuhan University. Published by Informa UK Limited, trading as Taylor & Francis Group.

This is an Open Access article distributed under the terms of the Creative Commons Attribution License (<http://creativecommons.org/licenses/by/4.0/>), which permits unrestricted use, distribution, and reproduction in any medium, provided the original work is properly cited. The terms on which this article has been published allow the posting of the Accepted Manuscript in a repository by the author(s) or with their consent.

C. Wang et al. 2025). This pronounced disparity has led to severe challenges in agricultural irrigation, industrial water supply and domestic water access in the north. For example, excessive groundwater extraction in the North China Plain has caused severe groundwater depletion, threatening long-term aquifer sustainability (Liu, Yu, and Kendy 2001; Fang et al. 2010; Foster et al. 2004). In contrast, southern China experiences frequent flooding due to abundant rainfall, while a substantial portion of its water resources remains underutilized (Lyu et al. 2018; C. Wang et al. 2022; Q. Zhang et al. 2017). In this context, addressing the imbalance between water resources in the north and south is not only a core challenge for water resource management but also a critical prerequisite for achieving sustainable socio-economic development across the country.

To mitigate the acute water scarcity in northern China, the South-to-North Water Diversion Project (SNWDP) was initiated. As the largest inter-basin water transfer project in the world, the SNWDP comprises three routes: the eastern, middle and western routes (Q. Zhang 2009). Among these, the Middle Route (MR-SNWDP) is the most prominent and strategically significant. Beginning at the Danjiangkou Reservoir on the Han River, the MR-SNWDP traverses Henan and Hebei provinces, ultimately delivering water to Beijing and Tianjin (Jia 2016; Y. Wang et al. 2023). Since the operation in 2014, the route has delivered more than 66 billion m<sup>3</sup> of freshwater to northern regions, significantly alleviating water shortages and enhancing water supply security (Green et al. 2015; Webber, Crow-Miller, and Rogers 2017). It has also benefited over 100 million people and bolstered economic and social development across northern China. Additionally, the project has contributed to environmental restoration, such as replenishing depleted rivers and improving groundwater levels (Jiang 2015; C. Zhang et al. 2020, 2021).

Scholars have extensively studied the MR-SNWDP from diverse perspectives, generating valuable insights while highlighting key challenges. Many studies have quantified the impacts of the project on water resources redistribution, demonstrating its vital role in reducing water scarcity and improving water security in northern China (Wei et al. 2010; C. Zhang et al. 2020). For example, hydrological models and remote sensing methods have shown significant improvements in water use efficiency and groundwater levels across the Beijing-Tianjin-Hebei region (Kattel et al. 2019; Long et al. 2020). Other investigations have examined the environmental effects of the project, including acceleration of vegetation greening, alterations in water quality, ecological changes in the Danjiangkou Reservoir and downstream ecosystem dynamics (S. Li, Li, and Zhang 2011; X. Li et al. 2024; J. Zhang et al. 2021). In addition, research has

emphasized the economic benefits of the water transfer, such as addressing disparities in water availability between urban and rural areas and supporting regional economic development (Wilson et al. 2017). Nevertheless, challenges associated with the implementation of the Middle Route have also been identified. The transfer of water has led to changes in hydrological patterns in the Water Source Areas (WSA), potentially reducing wetland areas and negatively impacting local biodiversity (Gu, Shao, and Jiang 2012; Q. Zhang et al. 2009). Furthermore, groundwater recharge in the Water Receiving Areas (WRA) has been slower than anticipated, raising concerns about the long-term sustainability of the intervention. Globally, other large-scale water diversion projects, such as the California State Water Project in the United States and the Interlinking of Indian Rivers program, provide valuable lessons regarding the potential benefits and risks of such undertakings (Das 2019; Grigg 2023).

Although many studies have explored the hydrological, ecological, and socio-economic effects of the MR-SNWDP, several critical limitations remained. Most research treated these aspects in isolation, lacking integrated analysis of their interactions and feedbacks. This fragmented approach limited understanding of how large-scale water transfers reshaped coupled natural-human systems over time. While some studies reported vegetation greening following the project's implementation, few quantitatively attributed these changes to specific drivers such as climate variability, water redistribution, or land use change (L. Li et al. 2015). The absence of robust attribution analysis hindered the identification of dominant factors influencing vegetation dynamics across different regions and time periods. Moreover, research mainly focused on the benefits of WRA, with limited attention to potential ecological trade-offs in the WSA (Long et al. 2020; S. Wang et al. 2024; Zou et al. 2016). Impacts such as reduced surface water storage and increased ecological vulnerability in the upper Danjiangkou watershed were often overlooked or insufficiently quantified. In addition, long-term and high-resolution evaluations of the project's cumulative effects remained scarce. Most existing studies relied on short-term datasets, lacking the temporal depth to detect delayed or non-linear environmental responses (Wilson et al. 2017; J. Zhang et al. 2021). Few studies assessed how vegetation recovery influenced urban microclimate or contributed to climate adaptation in receiving areas. These gaps underscored the need for a comprehensive and spatially explicit assessment that integrated multi-source data and addressed both ecological benefits and risks.

In this context, our study aims to provide a comprehensive understanding of the hydrological, ecological and climatic impacts of the MR-SNWDP on both the WSA and WRA from 2004 to 2023,

addressing key gaps in current research. The main objectives are: (1) to quantify the long-term hydrological effects of the project using Terrestrial Water Storage Anomalies (TWSA) data; (2) to evaluate the ecological impacts including the vegetation growing season and greening trends; (3) to separate the contributions of climate variability and human activities to vegetation dynamics; (4) to analyze the role of vegetation recovery in mitigating the urban heat island effect.

## 2. Data and methods

### 2.1. Study area

The MR-SNWDP is regarded as a landmark water conservancy project in China, developed to alleviate severe water shortages in northern regions by transferring water from water-abundant areas in the south. The project spans approximately 1432 km, originating from the Danjiangkou Reservoir on the Han River in central China and extending northward through cities in Henan and Hebei, ultimately supplying water to Beijing and Tianjin.

This study focuses on both the WSA and the WRA of the MR-SNWDP (Figure 1). The WSA include the cities of Hanzhong, Shangluo, Ankang and Shiyan, which are characterized by substantial water availability and ecological sensitivity. In contrast, the WRA encompass 20 cities, including Beijing, Tianjin and cities in Hebei and Henan provinces, where water scarcity has been exacerbated by high demand from agriculture, industry and urbanization. The regions exhibit significant spatial variability in topography and climate. The WSA are dominated by hilly and mountainous terrains and humid subtropical conditions, supporting dense forest ecosystems with high

vegetation coverage. In WRA, the landscape transitions into expansive plains with a temperate semi-arid climate, where vegetation primarily consists of cropland and grassland. These pronounced geographical and climatic differences underscore the necessity and challenges of inter-basin water transfers.

Year of 2024 marks the 10th anniversary of the MR-SNWDP, a historical milestone in water resource management in China. Over the past decade, the project has transferred over 66 billion m<sup>3</sup> of water to recipient regions, with Beijing and Tianjin receiving more than 10 billion m<sup>3</sup>, and Hebei and Henan benefiting from over 22 billion m<sup>3</sup>. This unprecedented scale of inter-basin water transfer has provided essential support for socioeconomic development and ecological restoration in northern China. Given the extensive water diversion, it is crucial to study the area in order to evaluate the socio-economic and hydro-ecological benefits for the WRA while quantifying the impacts on the WSA caused by water resources reallocation.

### 2.2. Data

The data products used in this study are shown in Table 1. The TWSA data was obtained from GRACE/GRACE-FO RL06.2 Mascon Solutions produced by the Center for Space Research (CSR) ([https://www2.csr.utexas.edu/grace/RL0602\\_mascons.html](https://www2.csr.utexas.edu/grace/RL0602_mascons.html)) (Ditmar 2018). The data collection was available from 2002 to 2023 at a monthly 0.25° resolution, which was calculated relative to the mean baseline from 2004 to 2010. The missing or anomalous GRACE data (17 months, 2011.01–2017.02) plus a 2-month gap in GRACE-FO (2 months, 2018.08–2018.09) and missing epochs (11

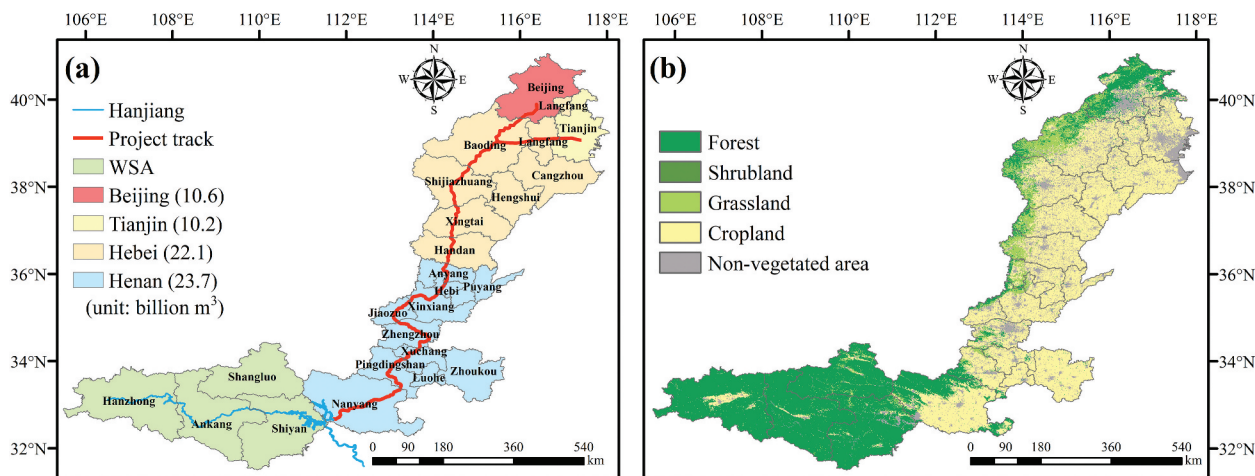


**Figure 1.** The study area for the satellite-based assessment of hydrological and ecological transformations from the MR-SNWDP. (a) Spatial distribution of the WSA, WRA and the main project track of the MR-SNWDP. The WRA include Beijing, Tianjin and cities in Hebei and Henan provinces. Numbers in parentheses indicate the total volume of water (in billion m<sup>3</sup>) transferred to each receiving region over the past decade. (b) Vegetation type distribution within the study area derived from satellite classification: forest, shrubland, grassland and cropland.

**Table 1.** The remote sensing and ancillary data products used for assessing hydrological and ecological transformations induced by the MR-SNWDP.

Product	Variable	Abbreviation	Spatial resolution	Temporal resolution	Period
CSR GRACE (RL06.2 Mascon)	Terrestrial Water Storage Anomaly	TWSA	0.25°	Monthly	2002–2023
MODIS NDVI (MOD13Q1 V6.1)	Normalized Difference Vegetation Index	NDVI	250 m	16 days	2000–2023
MODIS Land Cover Type (MCD12Q1 V6.1)	Forests Croplands Grasslands Built-up Lands Nighttime Lights Nighttime Lights Precipitation Evaporation Temperature_2m Wind Speed_10m	FOR CRO GRA BUI NL NL PRE EVA TMP WS	500 m 0.1°	Yearly Yearly 0.1° Daily	2001–2023 1992–2013 2014–2023 1950–2023
DMSP OLS (NOAA DMSP-OLS V4) VIIRS (NOAA VIIRS V1) ERA5-Land (ECMWF ERA5_LAND_MONTHLY_AGGR)	Terrestrial Water Storage Ground Water Storage Surface Soil Moisture Daytime Land Surface Temperature Global Artificial Impervious Area	TWS GWS SSM LST GAIA	0.25° 1000 m 1000 m	8 days	2003–2023
GLDAS-2.2 (NASA/GLDAS/V022/CLSM/G025/DA1D)					
MODIS Terra Land Surface Temperature and Emissivity (MOD11A2 V6.1)					2000–2023
Tsinghua FROM-GLC Year of Change to Impervious Surface (GAIA V10)					1985–2018

months, 2017.07–2018.05) were effectively addressed using the Singular Spectrum Analysis (SSA) gap-filling method (C. Wang et al. 2025; Yi and Sneeuw 2021).

The NDVI data was collected from MODIS Vegetation Indices (MOD13Q1 V6.1) (<https://lpdaac.usgs.gov/products/mod13q1v061/>) (Huete et al. 2002). The dataset spanned from 2000 to 2023, with a resolution of 250 meters and 16-day intervals, which was further synthesized into monthly products utilizing the Maximum Value Composite (MVC) method to remove the influence of cloud shadows and enhance seasonal signals (Holben 1986).

The daytime Land Surface Temperature (LST) data was obtained from the 8-day composite product MODIS Terra Land Surface Temperature and Emissivity (MOD11A2 V6.1), which eliminated the need for complex preprocessing steps, such as atmospheric correction (<https://earthdata.nasa.gov/data/catalog/lpccloud-mod11a2-061>) (Clinton and Gong 2013; Wan 2008). Due to the relatively stable variation in LST, this study focused exclusively on daytime LST values during the summer months of June, July and August. And the Global Artificial Impervious Area (GAIA) dataset was used to classify the urban and rural regions (<https://data-starcloudpcl.ac.cn/iearthdata/13>) (Kuang 2019).

The meteorological and hydrological data including Precipitation (PRE), Evaporation (EVA), Temperature (TMP) and Wind Speed (WS) data were derived from the ERA5-Land monthly dataset (<https://cds.climate.copernicus.eu/datasets/reanalysis-era5-land-monthly-means>) (Hersbach et al. 2020; Tarek, Brissette, and Arseneault 2020). The WS data was generated by combining the eastward and northward components of the 10 m wind. The other hydrological variables including Terrestrial Water Storage (TWS), Ground Water Storage (GWS) and Surface Soil Moisture (SSM)

were sourced from the Global Land Data Assimilation System (GLDAS) (<https://ldas.gsfc.nasa.gov/gldas/gldas-get-data>) (Rodell et al. 2004).

The variables utilized to assess the impact of human activities on NDVI included Built-up Lands (BUI), Croplands (CRO) and Nighttime Lights (NL) data. The BUI and CRO data were derived from the MODIS Land Cover Type Product, which originally classifies land into 17 categories (<https://lpdaac.usgs.gov/products/mcd12q1v061>) (Friedl et al. 2010). These categories were regrouped into four broader types: forests, croplands, grasslands, and built-up areas. The proportion of each type within grid cells was calculated to generate continuous variables representing land cover composition. BUI reflected urban expansion and impervious surfaces typically associated with vegetation loss, while CRO represented intensively managed agricultural areas influenced by human activities. The NL data was sourced from the two datasets: the Defense Meteorological Satellite Program – Operational Linescan System (DMSP-OLS) (<https://www.ngdc.noaa.gov/eog/dmsp>) (1992–2013) and the Visible Infrared Imaging Radiometer Suite (VIIRS) (2014–2023) (<https://www.ngdc.noaa.gov/eog/viirs>) (Elvidge et al. 2017; X. Li and Zhou 2017). The two datasets were normalized and merged to produce a continuous dataset covering the period from 2004 to 2023.

Other auxiliary data, including annual water usage by category (domestic, ecological, industrial and agricultural) for each province, was sourced from the Water Resources Bulletin (<http://szy.mwr.gov.cn/gbsj>).

### 2.3. Methods

The overall framework is presented in Figure 2. (a) Data collection and preprocessing: collecting datasets such as GRACE TWSA, MODIS NDVI, ERA5-Land,

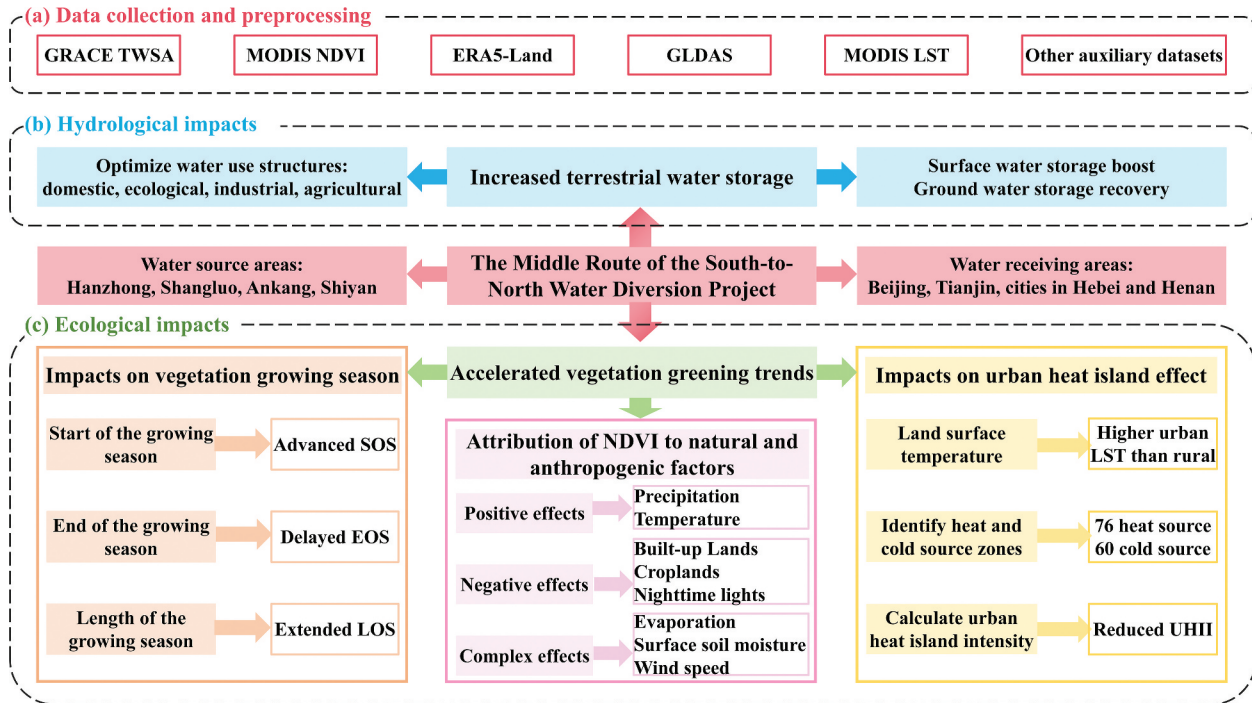


**Figure 2.** The overall framework for satellite-based assessment of hydrological and ecological impacts of the MR-SNWDP.

GLDAS, and conducting preprocessing operations; (b) Hydrological impacts in the WRA: highlighting increased surface water storage and groundwater recovery driven by water transfers from WSA to WRA, and exploring the water use structures; (c) Ecological impacts in the WRA: focusing on accelerated vegetation greening trends with changes in the growing season and reductions in urban heat island intensity, and attributing NDVI variations to natural and anthropogenic factors.

### 2.3.1. Trend analysis of TWSA and NDVI

In this research, we employed the Mann-Kendall (MK) test to assess the trends in TWSA and NDVI over the study period, which is a non-parametric statistical method widely used for detecting monotonic trends in time series data. The MK test is particularly robust against outliers and non-normally distributed data, making it well-suited for the long-term datasets used in this study (Mann 1945). The magnitude of the identified trends was quantified using Sen's slope estimator, and statistical significance was determined at the 95% confidence level (Sen 1968).

### 2.3.2. Extraction of vegetation growing season

Vegetation phenology, including cycles like bud break, flowering and senescence, is crucial for understanding vegetation-environment dynamics and its role in Earth system processes such as carbon and water cycles (Badeck et al. 2004; Richardson et al. 2013). Monitoring phenology helps assess interactions between vegetation and regional hydrological conditions, with metrics like the Start of the Growing

Season (SOS), End of the Growing Season (EOS), and the Length of the Growing Season (LOS) (Jeong et al. 2011; White et al. 2009). In this study, we utilized a 16-day NDVI time series spanning 2004 to 2023 to extract vegetation growing season dynamics.

Several methods were commonly used to extract vegetation growing season, including the threshold method, derivative method and inflection method (X. Zhang et al. 2003). The threshold method defined a fixed NDVI threshold to determine the growing season (Reed et al. 1994). The derivative method utilized the first or second derivative of the curve to identify changes in vegetation dynamics, such as the transition between green-up and senescence (X. Zhang et al. 2003). The inflection method examined changes in the curvature of the NDVI time series, marking key phenological events (Zeng et al. 2020). Moreover, the software tools have been developed to automate vegetation phenology analysis since 2000. TIMESAT used sigmoid curve fitting and smoothing techniques to model phenological events (Jonsson and Eklundh 2002). While reliable for high-quality data, it required extensive parameter tuning and manual intervention, especially in noisy datasets. Phenopix (Filippa et al. 2016) was designed for image-based phenology analysis, focusing on high-throughput processing of large datasets. However, it offered less flexibility in fine-tuning and handling contaminated points. Phenofit, developed by Kong et al. (2022), efficiently managed noisy data and complex seasonal variations and automated the extraction of growing season, making it well-suited for large-scale studies involving diverse vegetation types.

To extract growing season metrics, we adopt a mainstream multi-step approach based on the phenofit. First, quality control was applied to NDVI time series, assigning weights to pixels based on data reliability: 1 for high-quality data, 0.5 for cloud-contaminated data and 0.2 for missing data. This weighting system ensured the analysis relied primarily on reliable observations. Next, rough fitting methods were used to approximate seasonal vegetation dynamics. Representative approaches included the Savitzky-Golay filter for smoothing NDVI data and the Asymmetric Gaussian model for capturing growth patterns. After rough fitting, weights were updated using the Bisquare function to minimize outlier influence, while temporal smoothing adjusted weights based on seasonal consistency to accurately capture vegetation dynamics. Finally, precise phenological events were extracted using the first derivative method (Figure 3), which identified the SOS, EOS and LOS based on the rate of change in the NDVI time series.

### 2.3.3. Geographically weighted regression model for NDVI attribution

To further explore the driving factors of NDVI variability, we employed the Geographically Weighted Regression (GWR) model. Unlike traditional global regression models, GWR allows regression coefficients to vary spatially, enabling the capture of localized relationships between the dependent variable (NDVI) and its explanatory variables (Fotheringham, Brunsdon, and Charlton 2009). This is particularly advantageous for environmental and ecological studies, where spatial heterogeneity is often prominent.

The GWR model is an extension of the classical multiple linear regression model and can be expressed as (Brunsdon, Fotheringham, and Charlton 1996):

$$\text{NDVI}_i = \beta_0(u_i, v_i) + \sum_{k=1}^p \beta_k(u_i, v_i) X_{ik} + \varepsilon_i \quad (1)$$

where  $\text{NDVI}_i$  is the dependent variable at location  $i$ ,  $(u_i, v_i)$  is the spatial coordinates,  $\beta_0$  and  $\beta_k$  are the spatially varying intercept term and coefficients respectively, and  $\varepsilon_i$  represents the error term.

The spatial variability of the coefficients  $\beta_k(u_i, v_i)$  is determined by a kernel weighting function, which assigns higher weights to observations closer to the target location and lower weights to those farther away (Fotheringham, Brunsdon, and Charlton 2009). In this study, an adaptive Gaussian kernel was used to account for the spatial heterogeneity of vegetation-climate and vegetation-human interactions across the study area. The distance metric was determined by the number of nearest neighbors, with adaptive bandwidth selection optimized by minimizing the Akaike Information Criterion (AIC). The proximity of data points was determined based on the coordinate reference system, which facilitated accurate spatial distance calculations.

In this study, we conducted GWR attribution analysis for three key temporal points associated with the timeline of the MR-SNWDP: 2004 (prior to project implementation), 2014 (the year of project implementation) and 2023 (nearly a decade post-implementation). The explanatory variables incorporated in the GWR model were selected to capture both climatic and anthropogenic drivers of NDVI dynamics. Climatic variables included PRE, EVA, SSM, TMP and WS, which collectively represented the primary environmental controls on vegetation growth. Anthropogenic variables comprised BUI, CRO and NL, serving as a proxy for human activities and urbanization. To ensure the reliability of the GWR results, we assessed multicollinearity among explanatory variables using the

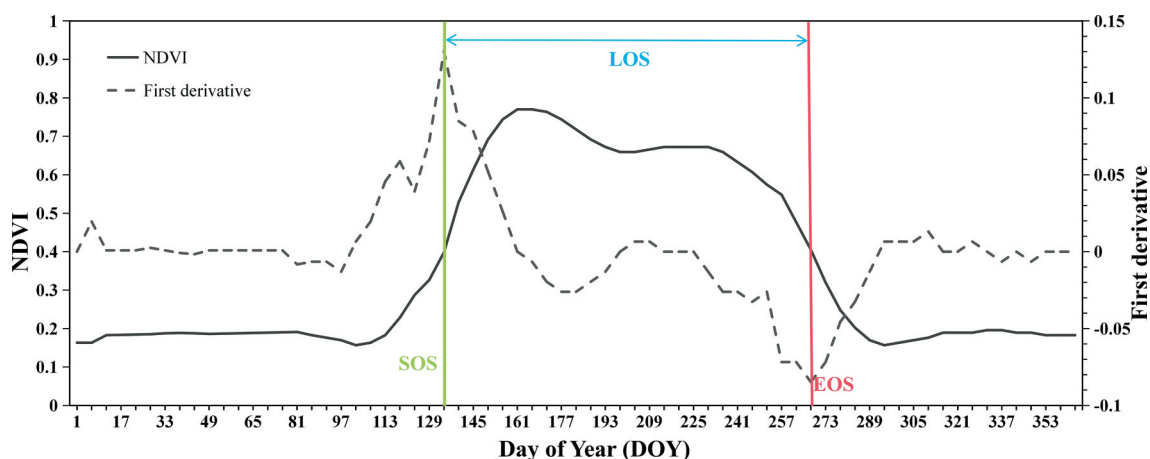


**Figure 3.** Schematic of vegetation growing season extraction using the first derivative method. The solid line represented the time series of the 16-day NDVI product, and the dashed line represented its first derivative. The day of year (DOY) corresponding to the maximum first derivative indicated the SOS, while the DOY corresponding to the minimum first derivative marked the EOS. The LOS is defined as the difference between EOS and SOS.

variance inflation factor, and tested for spatial autocorrelation of the dependent variable by calculating global and local Moran's I indices. And model performance was evaluated with several diagnostic metrics, including the Residual Sum of Squares (RSS), AIC and  $R^2$  values.

By focusing on the three specific years, we quantified the respective contributions of these drivers to NDVI variability, enabling a detailed analysis of how the relative influence of natural and human-induced factors evolved over time. This temporal segmentation allowed us to investigate vegetation dynamics before, during and after the project, revealing spatially explicit shifts in the primary factors influencing NDVI. This approach elucidated the nuanced interactions between vegetation dynamics, climatic fluctuations, hydrological conditions and anthropogenic interventions, offering a detailed perspective on the transformative ecological implications of the MR-SNWDP for regional vegetation systems.

### 2.3.4. Calculation of urban heat island intensity

In this study, we analyzed LST data to identify persistent heat and cold source zones and calculated Urban Heat Island Intensity (UHII). Long-term thermal anomalies were identified by applying a Gaussian filter to smooth the LST data, ensuring well-defined classification boundaries. Heat source zones were defined as pixels exceeding the 90th percentile of the annual LST distribution, while cold source zones fell below the 10th percentile. A pixel was classified as a persistent heat or cold source if it consistently met these criteria for at least 15 years within the 20-year study period (2004–2023). To ensure statistical significance, regions smaller than 10 contiguous pixels were excluded. The cumulative frequency of heat and cold source pixels over time was analyzed to identify areas with sustained extreme thermal characteristics. The classification for each pixel can be expressed as:

$$\text{Zone}(x, y) = \begin{cases} \text{Heat source zone, if } \sum_{t=2004}^{2023} 1(LST_{x,y}(t) > P_{90}(t)) > 15 \\ \text{Cold source zone, if } \sum_{t=2004}^{2023} 1(LST_{x,y}(t) < P_{10}(t)) > 15 \\ \text{Moderate zone, otherwise} \end{cases} \quad (2)$$

where 1 is the indicator function, returning 1 if the condition is true and 0 otherwise,  $LST_{x,y}(t)$  represents the average land surface temperature value at a specific pixel location  $(x, y)$  for a given year  $t$ ,  $P_{10}(t)$  and  $P_{90}(t)$  denote the 10th and 90th percentiles of the LST distribution for year  $t$ , respectively.

To calculate UHII, we integrated LST data with dynamic urban boundaries derived from GAIA. Annual GAIA datasets were applied to differentiate urban and non-urban areas, allowing urban boundaries to adapt to changes driven by urban expansion. For years beyond 2018, the urban boundary was fixed to the 2018 GAIA dataset. For each year, UHII was

quantified as the difference between the mean LST of urban and non-urban areas, ensuring that temporal urbanization dynamics and their thermal impacts on surrounding rural regions were captured (Kim 1992; L. Yang et al. 2016; Zhou, Zhang, Hao, et al. 2016). This integration of dynamic urban boundaries with long-term thermal anomaly identification provided an effective framework to assess the spatiotemporal evolution of the Urban Heat Island (UHI) effect.

## 3. Results

### 3.1. Spatiotemporal variations in TWSA and NDVI associated with the MR-SNWDP implementation

Since the opening of the MR-SNWDP in 2014, notable changes have been observed in the water resources and vegetation dynamics across the WSA and WRA. Using 2014 as the reference year, we analyzed the impacts on TWSA and NDVI, as shown in Figure 4. Before 2014, the study area exhibited a pronounced downward trend in TWSA, with a slope of  $-1.330$ . This decline was likely driven by urban expansion and the over-extraction of groundwater to meet increasing water demand, placing substantial pressure on water resources. However, after the opening, the rate of TWSA decline progressively slowed and TWSA began to show annual increases by 2020. This shift indicated the recovery of water resources, which benefited from the redistribution of water through the diversion project. In the WSA, TWSA remained stable before 2014, showing no significant changes. After the project began, TWSA exhibited a significant upward trend ( $\text{slope} = 0.619, p = 0.020$ ), suggesting improved water resource conditions despite outflows to the WRA. This improvement reflected water resource management and ecological restoration measures adopted in tandem with the project, as well as favorable precipitation conditions during the period. In contrast, the WRA experienced a sharp decline in TWSA prior to 2014 ( $\text{slope} = -1.874, p < 0.001$ ), indicating severe water scarcity caused by overextraction of groundwater and persistent droughts. Following 2014, TWSA shifted to an increasing trend ( $\text{slope} = 0.817$ ), although the change was not statistically significant. This recovery demonstrated the direct contribution of external water resources supply through the MR-SNWDP, which mitigated long-standing water deficits in the region.

Across the study region, NDVI exhibited a significant upward trend ( $\text{slope} = 0.00210$ ), showing sustainable improvements in vegetation cover and biomass. Following the implementation of the MR-SNWDP, the increase of NDVI in the WSA decelerated. The slowdown may highlight a reduction in water availability for vegetation growth due to water diversion. Despite this, NDVI continued to increase,

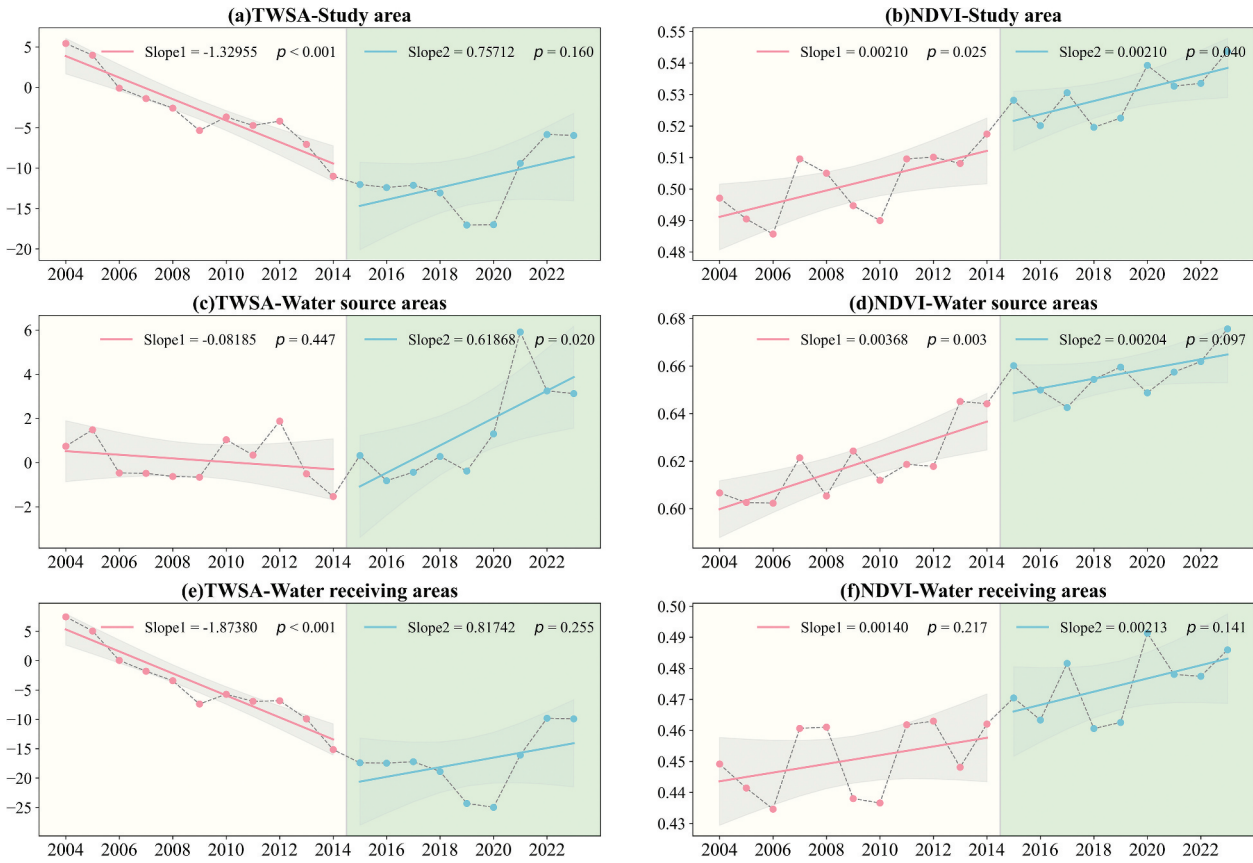


**Figure 4.** Annual trends of TWSA and NDVI before and after the MR-SNWDP implementation. Solid lines represented trends before (red) and after (blue) the project, with shaded areas showing the 95% confidence interval. The slopes indicated the magnitude of the trends, and the *p*-values reflected the statistical significance.

suggesting that ecosystem maintained vegetation productivity under changing hydrological conditions with strong resilience. In the WRA, NDVI experienced a marked acceleration after the initiation (slope increased from 0.00140 to 0.00213). This shift underscored the critical role of water availability as a limiting factor for vegetation recovery in these regions. The additional water supply through the MR-SNWDP significantly boosted vegetation growth,

particularly in drought-prone and ecologically fragile areas.

The changes in NDVI slope for each city before and after the MR-SNWDP are illustrated in Figure 5. The results revealed a significant increase in NDVI slopes across most WRA cities, reflecting improvements in vegetation growth and greening trends driven by enhanced water availability. Cities in Hebei Province, such as Shijiazhuang, Handan and Cangzhou, showed

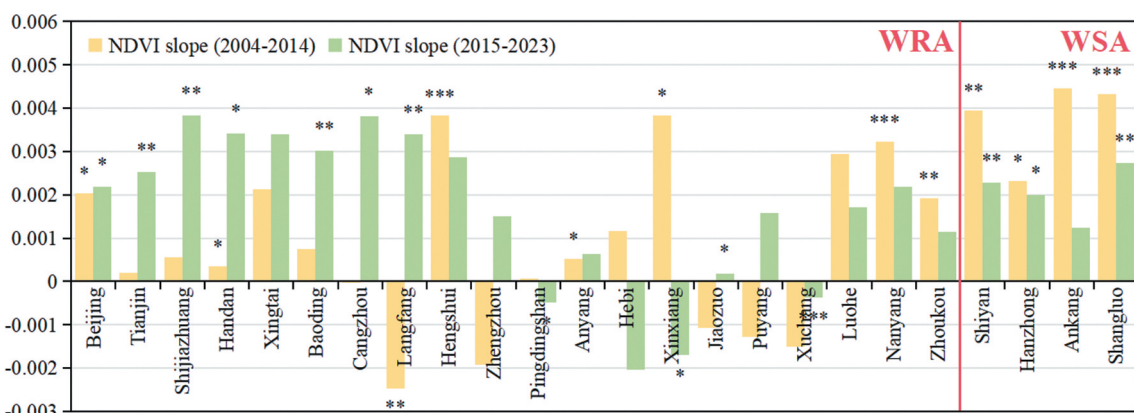


**Figure 5.** Vegetation greening trends (NDVI slope) before (yellow bars: 2004–2014) and after (green bars: 2015–2023) the MR-SNWDP implementation in WRA cities (first 20) and WSA cities (last 4). \*\*\*, \*\*, and \* represented significance levels of 1%, 5%, and 10%, respectively.

significant increases in NDVI slopes. This indicated that water supply alleviated water scarcity and provided sufficient irrigation for agriculture. Particularly notable were Langfang and Zhengzhou, where negative NDVI slopes before the project transitioned to positive slopes afterward. Moreover, slightly negative changes in NDVI slopes were exhibited in some cities, including Hebi, Zhoukou and Xinxiang. Ongoing pressures of urban development may have offset the anticipated benefits of improved water availability. The ecological influence of additional water resources on vegetation was inherently limited in highly urbanized areas. Meanwhile, the WSA cities experienced noticeable declines in NDVI slopes, reflecting the ecological trade-offs between localized vegetation growth and water resources redistribution to the north.

**Figure 6** illustrated the spatial distribution of annual trends in TWSA and NDVI, which highlighted significant shifts in TWSA within WRA following the implementation. Before the project, WRA showed a sharp decline in TWSA, reflecting severe water shortages. After 2014, over 80% of the WRA exhibited notable TWSA increases, indicating improved water availability. Nanyang and Luohe, continued to experience declines with persistent water resource challenges. Bar charts further confirmed this reversal, showcasing the effectiveness in alleviating water scarcity. Meanwhile, TWSA trends in WSA showed positive shifts, likely influenced by enhanced water management and favorable climate conditions. This

suggested that the MR-SNWDP not only redistributed water but also fostered more sustainable resource use in supplying regions. NDVI trends revealed significant greening across the study area. Prior to the project, WRA experienced slow vegetation growth due to limited water availability. After the implementation, greening areas increased from 55% to 64%, reflecting the ecological benefits of water supply in supporting vegetation and ecosystem recovery. In WSA, NDVI trends shifted notably between periods. Before the project, 80% of WSA exhibited significant greening, but this dropped to 45% afterward, suggesting that increased water stress from reallocation has led to slower vegetation greening and underscored the ecological costs of the diversion project.

### 3.2. Impacts of the MR-SNWDP on vegetation growing season

The MR-SNWDP has delivered significant volumes of water to Beijing and Tianjin. **Figure 7** showed the spatial distribution of vegetation growing season metrics before and after the diversion project, using Beijing as a case study. The enhanced water availability benefiting from this large-scale engineering initiative has notably influenced the growing seasons of local vegetation. In Beijing, vegetation was generally divided into three primary categories: forest, grassland and cropland. Forest was primarily distributed across the southwestern, northwestern and northeastern

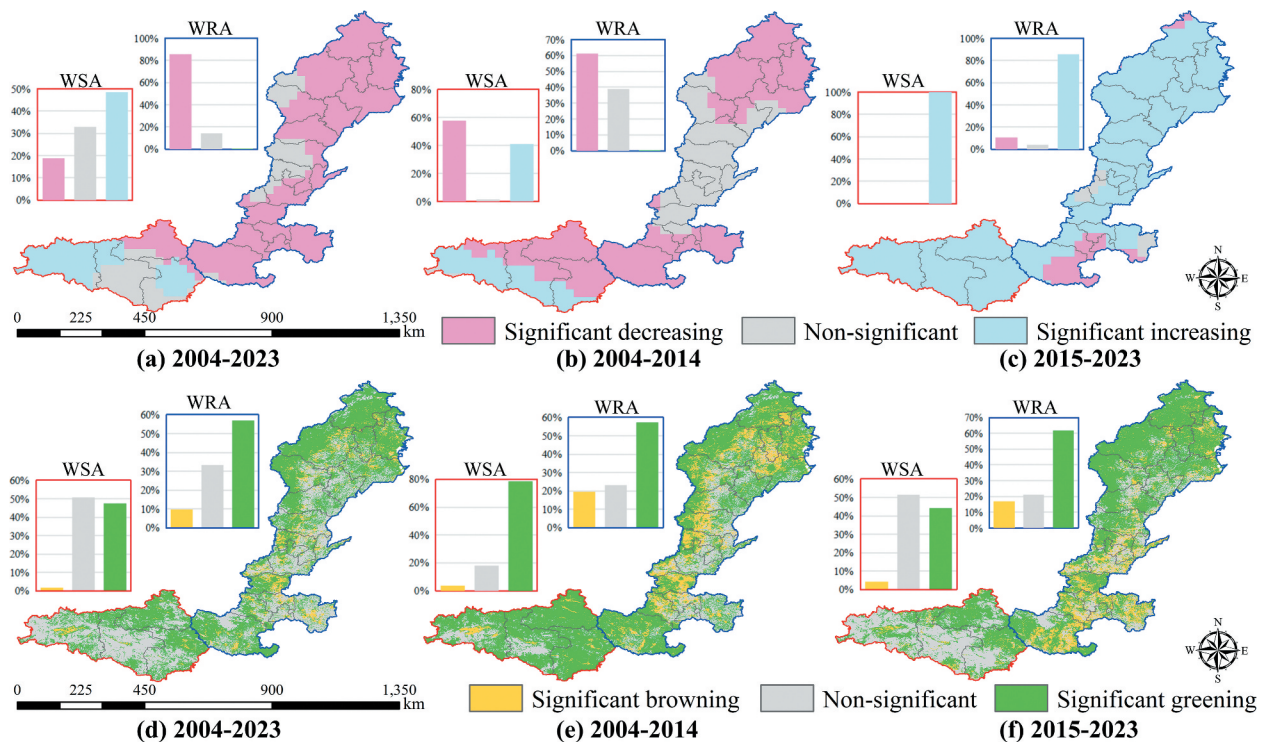


**Figure 6.** Spatial distribution of MK trends for TWSA (a, b, c) and NDVI (d, e, f) in the MR-SNWDP region. The analysis was divided into three periods. Red boundaries represented the WSA, and blue boundaries indicated the WRA. Bar charts showed the proportion of areas with different trend types, corresponding to the map legend.

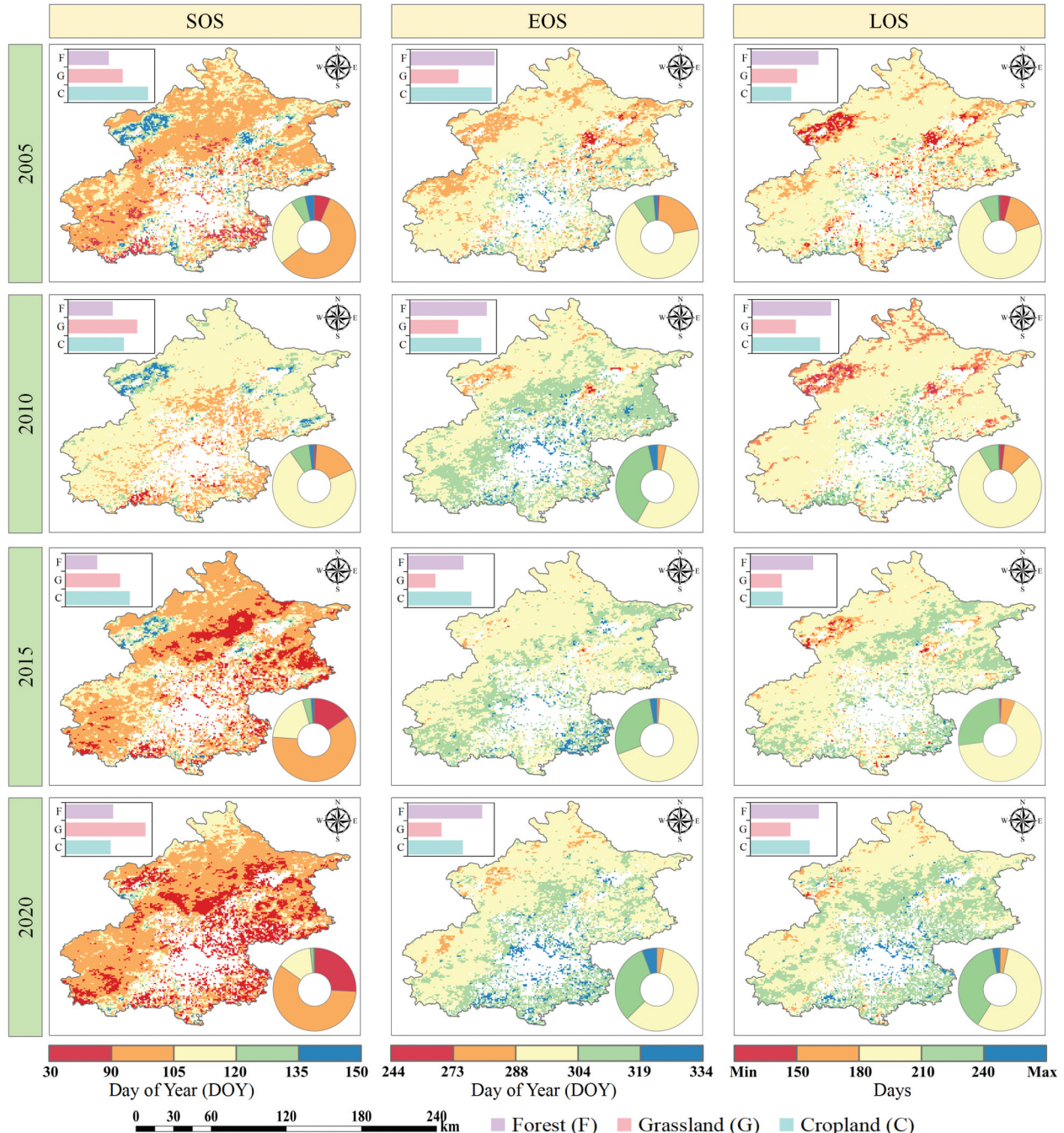


**Figure 7.** Spatiotemporal distribution of vegetation growing season metrics (SOS, EOS, LOS) in Beijing for the years 2005, 2010, 2015, and 2020. The white denoted the non-vegetation areas. The pie charts in the bottom-right corners displayed the proportion of areas covered by each category, while bar charts in the top-left corners presented the mean SOS, EOS and LOS for forest (F), grassland (G) and cropland (C).

regions of the city. Grassland was mainly concentrated in the western and northern areas, while cropland was predominantly located in the east and south.

In 2005, most vegetation in Beijing began growing including sprouting or flowering in early April (DOY 91–105). The leaf fall or senescence typically occurred in mid-to-late October (DOY 274–304), resulting in a growing season lasting approximately 5–7 months. By 2010, 75% of the vegetation indicated a delay in SOS with growth beginning in late April, which was roughly 15 days later than in 2005. Similarly, the EOS also delayed by about 15 days, shifting to early

November (DOY 305–319). Therefore, the LOS remained relatively stable, lasting 5 to 7 months. The observed delays in SOS and EOS in 2010 were largely attributed to water scarcity in Beijing, which limited vegetation growth in certain areas, particularly forest and grassland in northwestern city. These changes highlighted the sensitivity of vegetation phenology to water availability, underscoring the significant influence of environmental factors on growing season dynamics.

Following the commencement of the MR-SNWDP in 2014, vegetation phenology underwent obvious

changes. By 2015, SOS significantly advanced with 60% of vegetation initiating growth in early April (DOY 91–105), and 20% sprouting even earlier, prior to March. Compared to 2010, this represented a noticeable advancement at the start of the growing season. However, the EOS remained concentrated between mid-October to mid-November, resulting in a substantial increase in LOS. Notably, over 25% of vegetation sustained growth for more than 7 months. The forests in the northwest and northeast showed remarkable recovery, while croplands in the southeast exhibited extended growing durations due to improving water availability. This trend continued through 2020, with more than 80% of vegetation initiating growth before April 15th and EOS maintaining consistency around November. Consequently, the LOS was further extended, with 40% of vegetation sustaining growth for over 7 months annually. Particularly, the croplands in the central Beijing experienced enhanced productivity and prolonged growth periods, with some areas achieving nearly 8 months of continuous growth.

The observed phenological shifts underscored the critical role of the MR-SNWDP in alleviating water scarcity and improving vegetation dynamics in Beijing. The stable and consistent water supply over multiple years enabled forests and grasslands in the northwestern regions of Beijing to begin growing earlier (advanced SOS) and allowed croplands in the southeast to postpone the senescence (delayed EOS). As a result, the length of the growing season (LOS) for vegetation in Beijing increased significantly, indicating a clear trend of improved greening, which was consistent with Section 3.1. Notably, even regions where vegetation growth was previously constrained to less than 5 months, such as some forest areas in the west and east, experienced an extension of LOS to 7 months or more. This demonstrated the substantial impact of the water diversion project in promoting vegetation growth and stability across diverse ecological zones, achieving a remarkable improvement in the overall vegetation phenology and greening trends.

The response of different vegetation types to water diversion further elucidated the patterns. From the bar chart in Figure 7, it was evident that forests generally started growing earlier (the smallest SOS) and ended growth later (the largest EOS) compared to grasslands and croplands. This meant forests had a significantly longer growing season (LOS) than the other two vegetation types, as the perennial nature allowed them to access deeper soil moisture and nutrient reserves. Additionally, forests were less dependent on seasonal agricultural irrigation or surface water availability, which enabled them to start growing earlier in spring and sustain growth later into autumn. In comparison, croplands also exhibited a longer LOS than grasslands, primarily due to the later EOS. The croplands in Beijing consisted mainly of irrigated (81.93%) and rain-

fed (17.48%) cropland, which were concentrated around urban areas, allowing the crops to benefit from greater access to water supply from the project. By 2020, croplands in Beijing demonstrated a notable advancement in the SOS compared to 2010, where the vegetation began growing as early as February, and the EOS extended into November. In particular, the areas closest to central Beijing experienced the most dramatic improvements, with some vegetation sustaining growth for nearly 10 months. These changes underscored the critical role of water resource management in optimizing vegetation growth and extending growing periods across diverse vegetation types in Beijing.

The temporal variations in the average LOS for vegetation across different regions and vegetation types were represented in Figures 8 and 9, respectively. The results revealed that the MR-SNWDP had a significant impact on the growing season length in the WRA. From 2004 to 2023, LOS in Beijing, Tianjin, and Hebei showed steady and significant increases, rising from approximately 200 days in 2004 to around 220 days in 2023. This upward trend reflected improvements in water availability that mitigated drought stress, enabling earlier vegetation growth (SOS) and delayed senescence (EOS), particularly in agricultural and forested regions. After 2014, the rate of LOS increases in these regions accelerated significantly, with the annual growth rate in Beijing rising from 1.41 to 1.72 days/year, while Tianjin and Hebei both saw increases of about 0.35 days/year. Although the LOS trend in Henan increased from -2.08 to 1.78 days/year, the change was not statistically significant. In the WSA, the LOS trend remained relatively stable, with a slight decline from 0.58 to 0.55 days/year. However, the vegetation exhibited substantial interannual fluctuations in LOS, particularly during 2017, 2020 and 2022, when the LOS shortened sharply. These fluctuations reflected increasing sensitivity of the local ecosystems to climatic variability, as large-scale water diversion may have altered regional hydrological and ecological stability. Different vegetation types also displayed distinct trends. Forests maintained the largest and most stable LOS (220–235 days) due to the ecological resilience, while grasslands experienced a consistent increase of 0.6 days/year. Croplands showed the most pronounced changes, with LOS trend increasing from -0.20 to 2.23 days/year after 2014, reflecting the direct benefits of enhanced agricultural irrigation water. Moreover, the vegetation LOS in the WSA reached up to 250 days, exceeding that of the WRA due to its predominantly forested landscape.

### **3.3. Attribution of NDVI to natural and anthropogenic factors**

Before analyzing the spatially varying effects of natural and anthropogenic factors on NDVI using the GWR

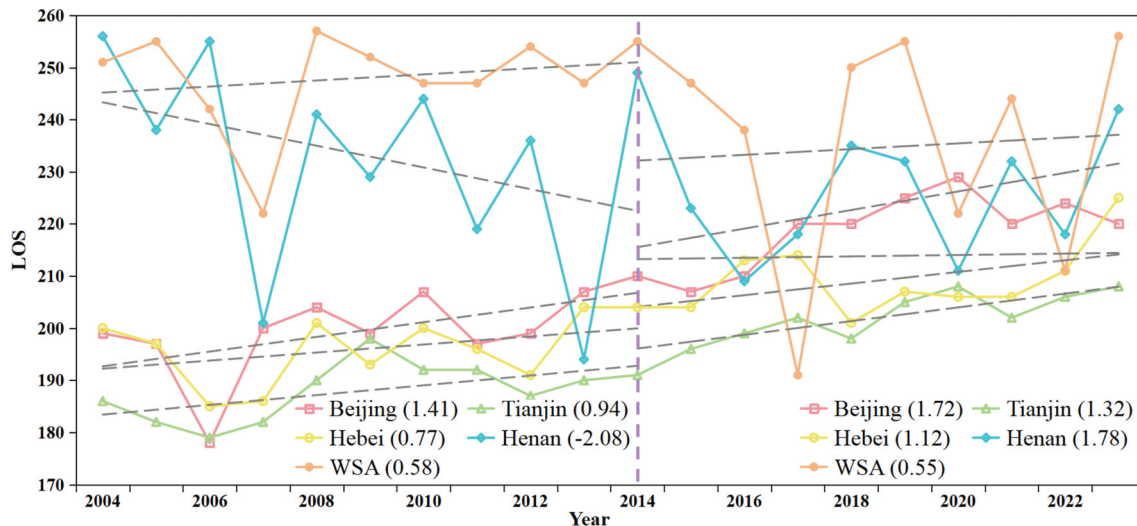


**Figure 8.** Temporal trends in vegetation growing season length (LOS) across the WSA and WRA of the MR-SNWDP from 2004 to 2023. Numbers in parentheses indicated the slope. Gray dashed lines showed linear trend fits for each region.

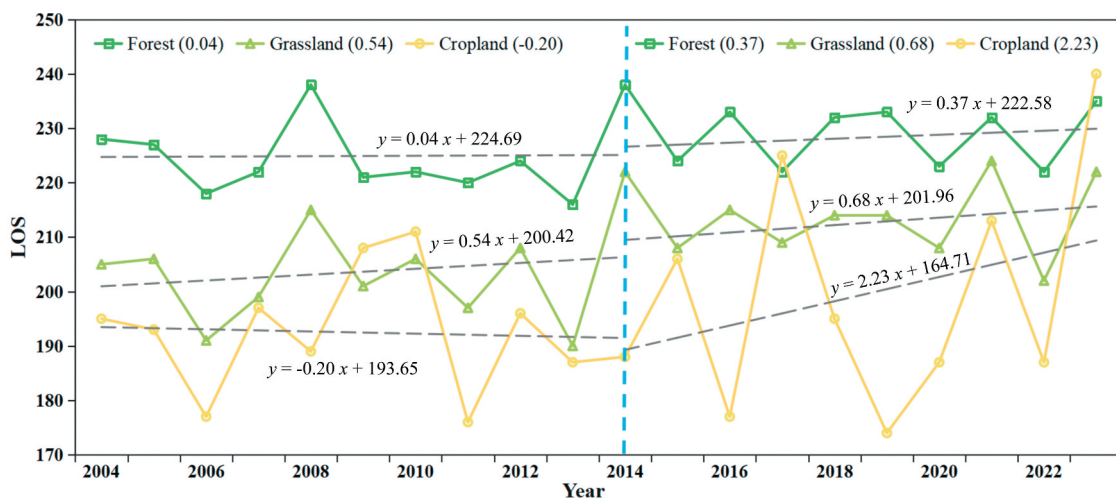


**Figure 9.** Temporal trends in vegetation growing season length (LOS) for different vegetation types in the WRA of the MR-SNWDP from 2004 to 2023. Numbers in parentheses indicated the slope. Gray dashed lines showed linear trend fits to each vegetation type.

model, we conducted spatial autocorrelation tests to confirm the presence of spatial dependence in the dependent variable. The global Moran's I values for NDVI in 2004, 2014, 2023 (Appendix Table A1) were consistently high ( $I > 0.89$ ,  $p < 0.001$ ), indicating strong and statistically significant positive spatial autocorrelation. Local Moran's I analysis (Appendix Figure A1) further revealed clear spatial clustering, with high-high NDVI clusters concentrated in the southern regions and low-low clusters in the north, confirming the presence of spatial heterogeneity and justifying the use of the GWR model. To ensure the reliability of the GWR results, we also assessed multicollinearity among the independent variables using the Variance Inflation Factor (VIF). As shown in Table 2, all variables across the three years had VIF values below the commonly accepted threshold of 5, indicating no multicollinearity. Furthermore, all explanatory variables were normalized before

regression analysis, and the standard deviations after normalization were consistently below 0.3, suggesting that the input data were well scaled and suitable for comparing coefficient magnitudes across variables.

Table 2 also presented the mean GWR regression coefficients of the selected driving factors. Three anthropogenic factors exhibited consistent negative effects on NDVI, BUI had the strongest suppressive impact ( $-0.182$ ) followed by CRO ( $-0.105$ ) and NL ( $-0.072$ ). This suggested that urban expansion and increased impervious surface coverage played a dominant role in reducing vegetation greenness, while NL captured indirect effects associated with urbanization, population growth and socioeconomic development, which had relatively smaller but persistent negative influences on vegetation. For climatic variables, PRE and TMP consistently showed positive associations with NDVI, highlighting the fundamental role in supporting plant growth. Sufficient rainfall

**Table 2.** The VIF, standard deviation and mean GWR regression coefficient of driving factors for 2004, 2014, 2023.

Year	Factors	BUI	CRO	NL	PRE	EVA	SSM	TMP	WS
2004	VIF	3.118	3.923	3.061	2.634	2.887	1.905	3.458	2.043
2014		3.053	4.885	2.576	4.317	4.702	3.256	2.324	2.193
2023		2.464	3.865	2.487	4.384	3.233	2.893	3.097	2.209
2004	standard deviation	0.133	0.282	0.183	0.193	0.174	0.198	0.17	0.183
2014		0.142	0.284	0.176	0.181	0.202	0.191	0.186	0.185
2023		0.141	0.275	0.241	0.219	0.236	0.201	0.194	0.171
2004	mean GWR regression coefficient	-0.148	-0.049	-0.041	0.069	-0.077	-0.016	0.101	-0.020
2014		-0.114	-0.094	-0.097	0.304	0.098	-0.034	0.058	0.014
2023		-0.182	-0.105	-0.072	0.086	-0.081	-0.023	0.056	-0.012

increased soil water availability, while warmer temperatures enhanced photosynthetic efficiency and extended the growing season. Conversely, SSM displayed a persistent negative effect on NDVI. The effects of EVA and WS were more complex, exhibiting a non-linear pattern that strengthened before diminishing. Moderate EVA may support transpiration and cooling, while excessive EVA indicated water stress. Similarly, WS may promote gas exchange at low levels but can lead to erosion and plant damage when high. Throughout the study period, anthropogenic pressures on vegetation have intensified, whereas the positive influences of natural factors were insufficient to offset this trend during the MR-SNWDP implementation.

The spatial distribution of regression coefficients based on the GWR model is shown in Figure 10. In 2004, human activities predominantly contributed to a decline in NDVI, with considerable spatial variability across cities, as illustrated in Figure 10(a). Urban expansion exerted widespread ecological stress, particularly in highly urbanized cities like Beijing, Zhengzhou and Jiaozuo, where BUI exhibited a strong inhibitory effect on vegetation growth. This underscored the destructive impact of land development and impervious surface expansion on ecosystems under conditions of severe water stress. CRO exhibited a positive effect on NDVI in cities with extensive agricultural land use, such as Anyang, Zhengzhou and Xinxiang, where cropland supported stable vegetation coverage through managed planting activities. In contrast, negative impacts of CRO appeared in cities like Beijing and Baoding, where land use was dominated by urban infrastructure. The influence of NL was relatively minor in most cities but showed notable negative effects in Baoding and Nanyang, reflecting localized pressure from socioeconomic development and population aggregation. For climate factors, PRE and TMP showed positive effects on NDVI in WRA like Anyang, Hebi and Shijiazhuang, while exhibited negative effects in Beijing, Tianjin and Nanyang. Other climate variables including SSM and WS showed negative effects in most cities. Meanwhile, vegetation NDVI in WSA was more strongly affected by human factors such as BUI and CRO rather than natural climatic variables.

Before the project, the relatively healthy ecosystems in WSA were not significantly constrained by environmental limitations, but were instead impacted by human-driven land use changes including urban expansion and farmland conversion.

In 2014, the year the MR-SNWDP was launched, the GWR model revealed significant changes in the spatial distribution of the positive effects of climate factors and the negative impacts of human activities on NDVI (Figure 10(b)). The negative effects of BUI and CRO in Beijing, Anyang and Hebi were somewhat alleviated, indicating a reduction in water stress and an improvement in ecosystem resilience. Climate factors such as PRE, TMP and EVA exhibited positive effects on NDVI across most cities in the WRA, indicating that favorable climatic conditions, including increased rainfall, warmer temperatures and moderate evaporation, have contributed to improved vegetation growth and ecosystem health in these regions. However, SSM showed negative effects on NDVI in cities of Henan Province, possibly due to inefficient water use, while it showed positive impacts in Hebei Province, where soil moisture was a limiting factor in 2004. Notably, in the WSA, the negative influence of BUI was weakened compared to 2004. In contrast, the negative impact of NL significantly increased, especially in Shiyan and Hanzhong, indicating growing socioeconomic activity and associated ecological pressures in the region. In 2014, natural climatic factors emerged as the dominant drivers of vegetation dynamics, while the relative negative influence of human activities diminished.

In 2023, a decade after the launch of the MR-SNWDP, the long-term ecological effects became more evident and stable across the region, as represented in Figure 10(c). The negative impacts of BUI and CRO became more pronounced, especially in Baoding, Xinxiang and Hanzhong. This trend suggested intensified urban expansion and increased anthropogenic disturbances to cropland, reflecting the ongoing acceleration of urbanization and agricultural land modification. Meanwhile, the positive influences of PRE and TMP on NDVI weakened compared to 2014. This was attributed to the long-term redistribution of water resources following the implementation of the MR-SNWDP, which alleviated water scarcity and rendered vegetation growth less sensitive

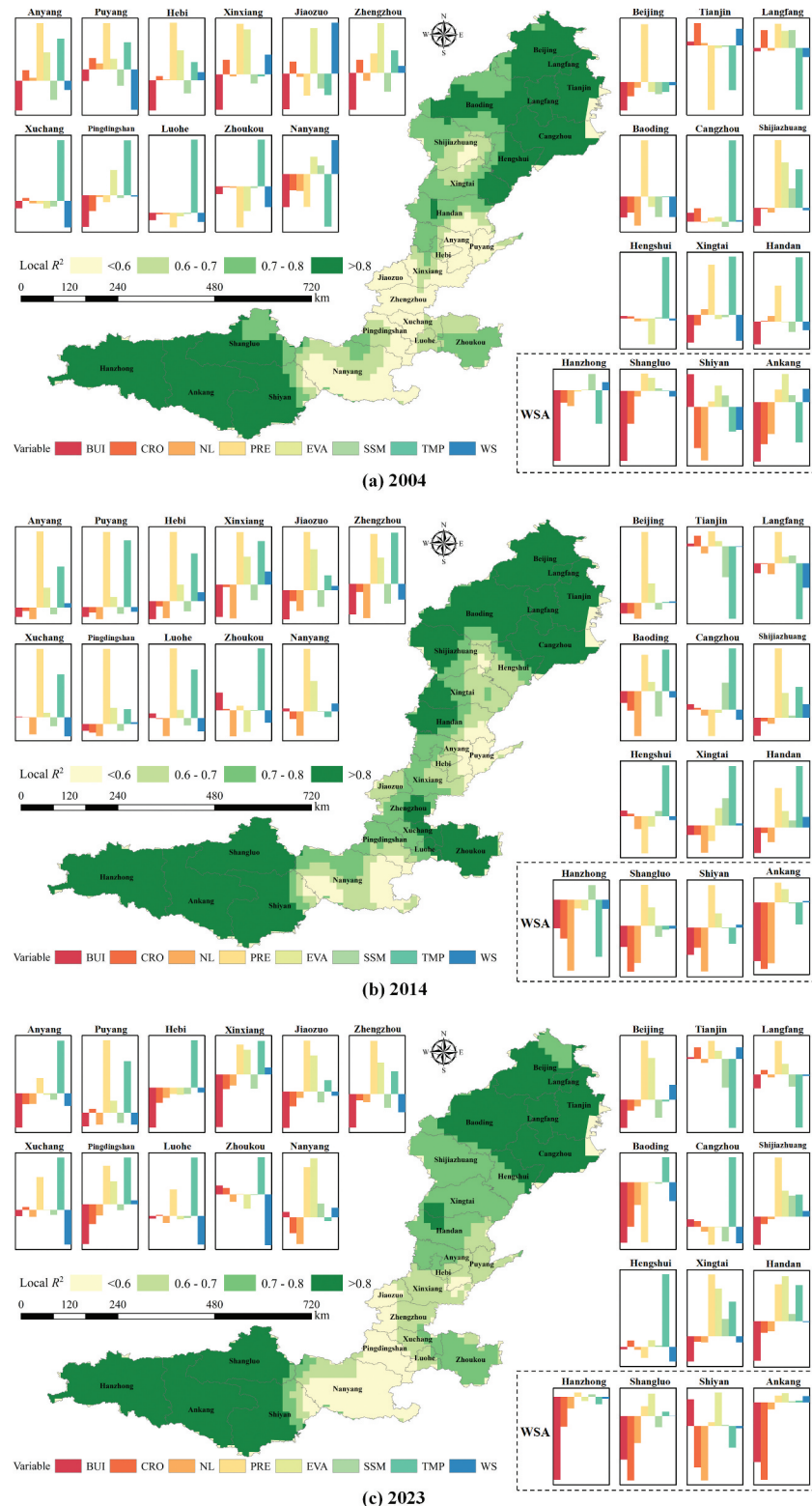


**Figure 10.** Distribution of regression coefficients of driving factors influencing NDVI based on the GWR model. The green base map showed the spatial distribution of the local  $R^2$  values from the GWR model. The bar charts around the map represented regression coefficients of 8 factors for 24 cities.

to climatic fluctuations. Overall, the combined effects of climatic and anthropogenic factors on NDVI in the WRA were mostly positive, suggesting that improved water availability and ecological restoration efforts have supported vegetation recovery in these areas. In contrast, the WSA exhibited predominantly negative effects, where vegetation was less influenced by

climatic variability but increasingly impacted by human interventions.

The GWR model demonstrated strong performance in the study area, with local  $R^2$  values exceeding 0.8 in key cities, such as Beijing, Tianjin and Langfang. This reflected the stability of the ecosystems and the predictable influence of driving factors on NDVI

**Table 3.** Comparison of accuracy metrics for global regression and GWR model.

Year	Global Regression				Geographically Weighted Regression			
	AIC	RSS	$R^2$	Adjusted $R^2$	AIC	RSS	$R^2$	Adjusted $R^2$
2004	-3266.261	4.969	0.582	0.579	-4231.685	2.636	0.828	0.788
2014	-3096.466	5.073	0.666	0.664	-4107.189	3.351	0.868	0.829
2023	-3375.867	5.066	0.707	0.705	-4084.411	2.944	0.848	0.816

changes. In contrast, cities in Henan Province, such as Puyang and Nanyang, exhibited local  $R^2$  values below 0.6 across the three stages. The ecological changes in these regions were influenced by more complex and multifaceted factors that the model could not fully capture. We compared the model performance and found that GWR outperformed global regression by better capturing spatial heterogeneity, as shown in Table 3. GWR consistently achieved lower AIC and RSS values, indicating a better model fit and reduced residual errors. Additionally, GWR showed higher  $R^2$  and adjusted  $R^2$  values, reflecting stronger explanatory power.

These results clearly revealed the dynamic and heterogeneous changes in NDVI across the study area, driven by both human activities and climate factors within the timeline of the MR-SNWDP. Human activities, particularly BUI and CRO, had a significant negative impact on NDVI, while climate factors, especially PRE and TMP, served as key drivers of vegetation greening. The project played a crucial role in alleviating water stress and promoting vegetation greening in WRA, which reduced the impacts of climatic fluctuations on vegetation and enhanced ecosystem resilience. Additionally, the MR-SNWDP contributed to restoring ecological balance by improving water availability in drought-prone regions and fostering a sustainable water-ecosystem feedback loop.

### 3.4. Impacts of the MR-SNWDP on urban heat island effect

The WRA of the MR-SNWDP have exhibited an evident greening trend over the past two decades. Previous studies have demonstrated a strong correlation between vegetation cover and surface temperature (Peng et al. 2014; Weng, Lu, and Schubring 2004). In this study, Figure 11 presented the regression relationships between NDVI and LST in the WRA, reflecting the role of vegetation cover in regulating surface temperature across both spatial and temporal dimensions. Across three selected years (2004, 2014, and 2023), a statistically significant negative correlation was observed between NDVI and summer daytime LST, indicating that higher vegetation density was consistently associated with lower surface temperature. Among the four regions, Beijing exhibited the strongest relationship, with a correlation coefficient close to -0.70 and a regression slope of approximately -25, reflecting the substantial cooling effect of dense

vegetation (NDVI values primarily between 0.4 and 0.7). In contrast, Tianjin demonstrated the weakest correlation, due to limited vegetation cover, with NDVI values concentrated between 0.3 and 0.5. The 95% confidence ellipses represented the uncertainty and dispersion of the data, with tighter ellipses indicating a more stable vegetation-temperature relationship. Importantly, the temporal comparison revealed that increases in NDVI from 2004 to 2023 in cities such as Beijing and Henan were accompanied by reductions in LST. This trend suggested that vegetation greening played an important role in mitigating urban thermal conditions.

Building on the NDVI-LST relationships, our study investigated whether the significant ecological improvements driven by the project have mitigated the UHI effect in these regions. Figure 12 illustrated the spatiotemporal dynamics of summer daytime LST in the WRA, revealing significant regional disparities, urban-rural contrasts and long-term trends from 2004 to 2023. The spatial distribution of LST highlighted a clear east-west dichotomy with average LST of 32.73°C, as shown in Figure 12(a). High-temperature zones, reaching up to 41.37°C, were concentrated in densely populated urban areas in the east, where intensive human activities and built-up landscapes amplified the UHI effect. In contrast, the western regions dominated by forests and grasslands displayed significantly lower temperature with a minimum of 20.46°C, reflecting the regulatory role of vegetation in mitigating surface heat. This spatial pattern was further reinforced by the identification of long-term cold and heat source zones between 2004 and 2023. Cold sources were predominantly located in areas with dense vegetation cover, where LST values remained below the 10th percentile for 15 consecutive years. In contrast, heat sources were concentrated in urban centers and industrial zones, with LST values consistently exceeding the 90th percentile, driven by the intensifying impact of urbanization. This interplay between natural ecosystems and urban development highlighted the critical need for preserving natural cold source zones to mitigate the thermal stress caused by expanding urban heat source zones.

The comparison of urban and rural LST further highlighted the warming effect of urbanization in the WRA. The box plots in Figure 12(a) indicated that urban LST consistently ranged from 32°C to 34°C, while rural LST ranged from 29°C to 31°C, resulting in an average temperature difference of

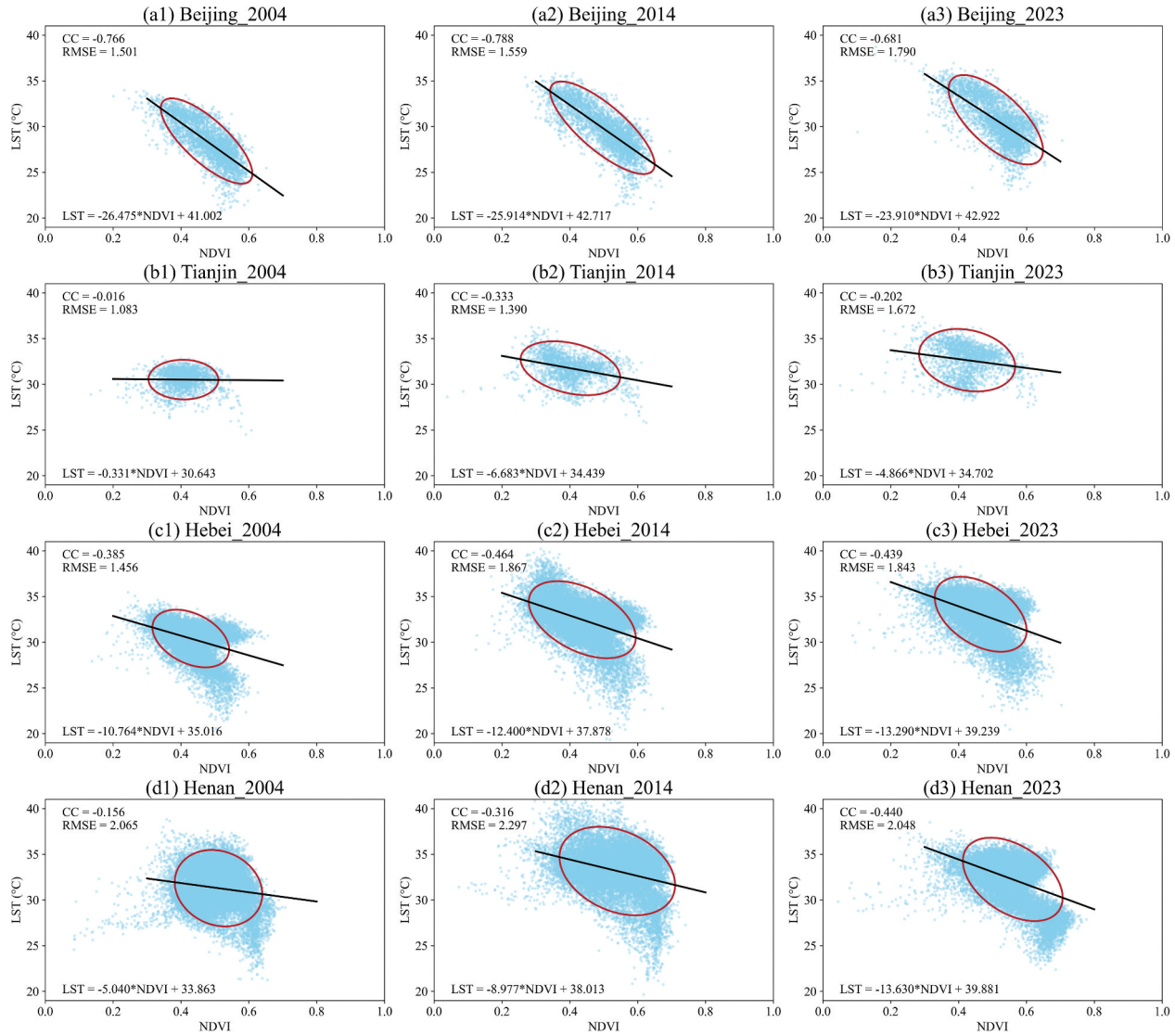


**Figure 11.** Scatter plots and regression relationships between NDVI and summer daytime LST in the WRA for 2004, 2014, and 2023. Each subplot showed scatter points, linear regression lines, Correlation Coefficients (CC), Root Mean Square Error (RMSE), and regression equations (slope and intercept). The ellipses represented 95% confidence intervals of the data distribution, capturing the spatial variability of NDVI-LST relationships.

3°C across the entire region from 2004 to 2023. Specifically, Beijing exhibited the most pronounced disparity, with the urban-rural temperature difference reaching up to 5°C. This finding reflected the high density of built-up areas and intense anthropogenic activities, which significantly amplified the UHI effect. In contrast, Tianjin, Hebei and Henan showed smaller urban-rural temperature gaps of approximately 2°C, potentially due to lower urbanization levels or better preservation of natural landscapes. Notably, the box plots revealed anomalously low rural LST values in 2021, particularly in Beijing and Tianjin. These localized cooling may be attributed to specific climatic conditions or changes in land use, such as increased precipitation or expanded vegetation cover. Further investigation into these anomalies could deepen our understanding of short-term climatic variability and its impact on LST, providing valuable insights for developing

more targeted and adaptive urban climate strategies.

The changes in UHII based on summer LST in the WRA of the MR-SNWDP are illustrated in Figure 13. By comparing UHII trends before and after the project operation, the results revealed its influence on regional climate regulation and the differing patterns of urbanization and ecological recovery across the provinces. Beijing experienced the most significant reduction in UHII after the implementation of the project. Before 2014, UHII displayed a positive trend with a slope of 0.114, indicating a consistent annual increase in heat intensity. After 2014, this trend shifted dramatically with the slope decreasing to -0.057. At the same time, the UHII slope of Hebei decreased by 0.013°C annually, while Henan experienced a more substantial annual reduction of 0.038°C. These notable changes demonstrated the effectiveness of the MR-SNWDP in mitigating UHI effect. Enhanced water availability

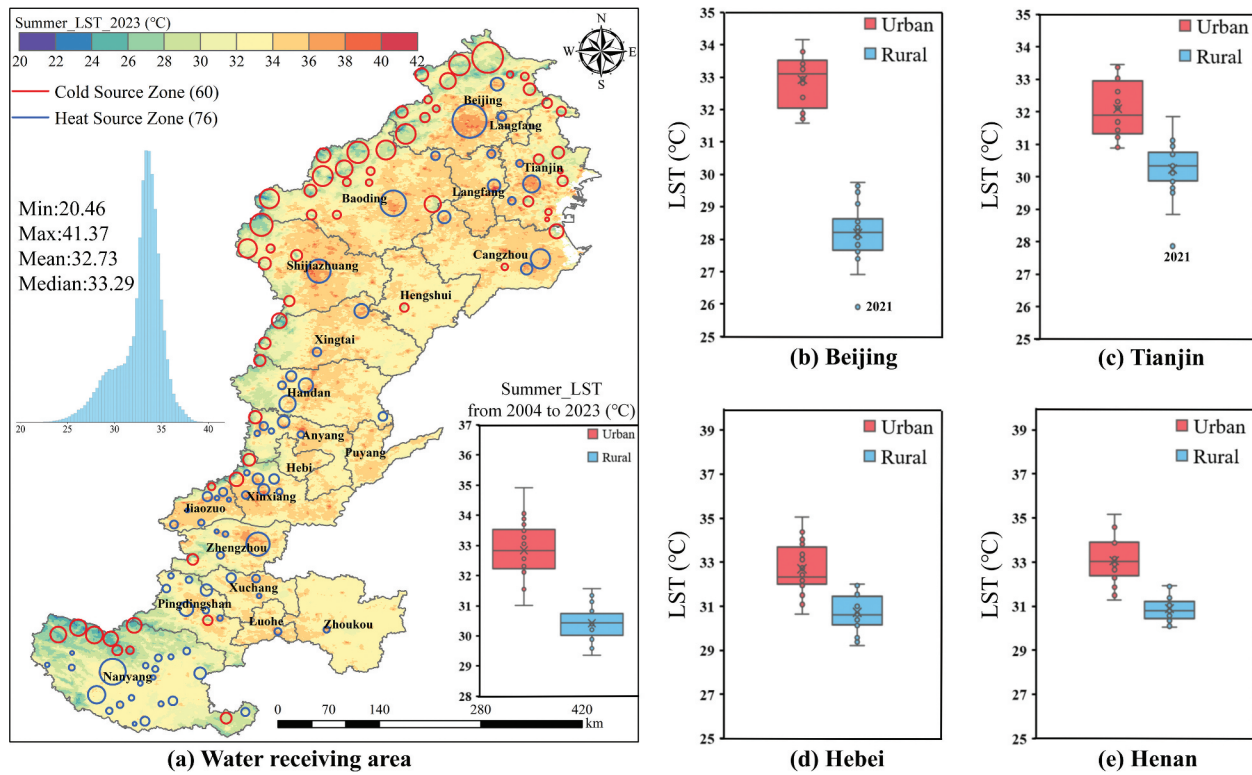


**Figure 12.** Distribution and changes in summer daytime LST in the WRA from 2004 to 2023. (a) Exhibited the distribution of average LST in 2023 with identification of cold and heat source zones. Red circles represented cold source zones and blue circles represented heat source zones, with circle sizes corresponding to the number of pixels in each region. A total of 60 cold source and 76 heat source zones were identified, excluding those with fewer than 10 pixels. The histogram on the left showed the distribution of LST in 2023. (b)–(e) Box plots showed the urban and rural average LST from 2004 to 2023 for Beijing, Tianjin, Hebei, and Henan, respectively.

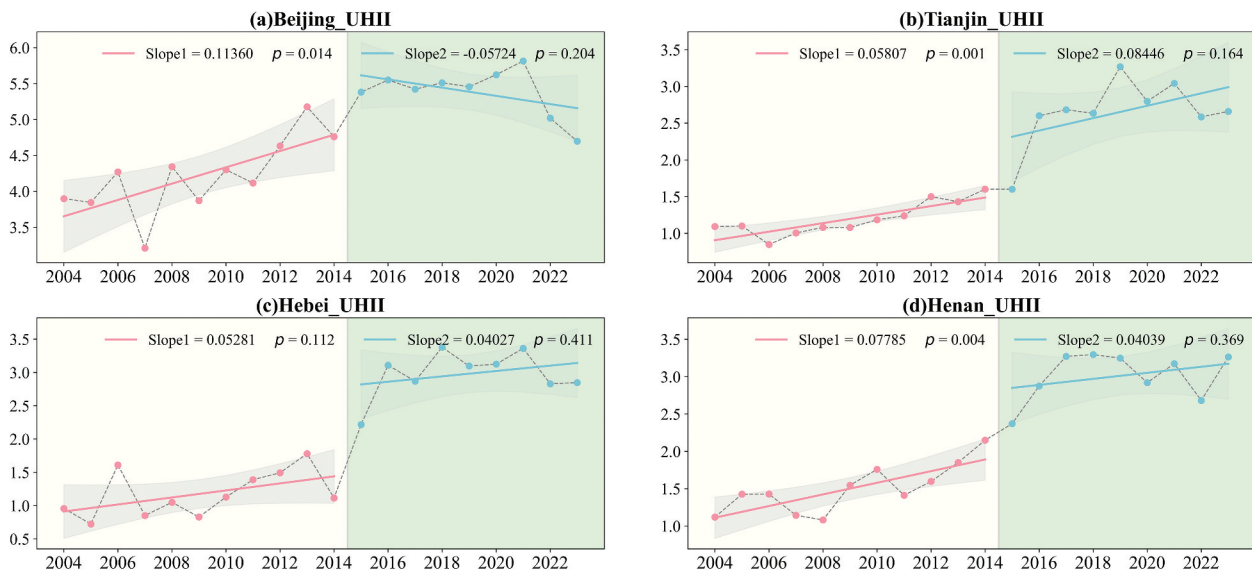


**Figure 13.** Annual trends of UHII before and after the MR-SNWDP implementation in the WRA. Solid lines represented trends before (red) and after (blue) the project, with shaded areas showing the 95% confidence interval. The slopes indicated the magnitude of the trends, and the  $p$ -values reflected the statistical significance.

enabled extensive greening efforts in these areas, which strengthened the ability of the ecosystem to regulate surface temperatures. However, Tianjin exhibited an increase in UHII following the project. The UHII slope increased from 0.058 to 0.084, reflecting an intensification of urban heat conditions. This

upward trend can be contributed to its consistently low NDVI values (0.34–0.38), which indicated insufficient greening to offset the intensifying heat. This disparity underscored the essential role of vegetation in regulating urban thermal environments and highlighted the urgent need for Tianjin to enhance

greening efforts in its urban planning to address escalating thermal stress. Furthermore, a significant increase in UHII across the four provinces was observed between 2014 and 2016. Large-scale construction activities and intensified human activity during the initial phase of the project, including surface disruptions and energy consumption, likely contributed to a temporary amplification of UHI effect.

## 4. Discussion

### 4.1. Surface water storage dominance in project impacts

The MR-SNWDP had a significant spatiotemporal impact on water resource distribution and ecological restoration in the WRA, reflecting the profound changes human intervention has brought to natural hydrological dynamics (Kattel et al. 2019; Long et al. 2020). As shown in Figure 14, the changes in SWS and GWS between 2004 and 2023 exhibited significant spatial heterogeneity. The project had notably increased SWS in Beijing and Tianjin, serving as the primary driver behind the rise in TWS. Since the initiation of water diversion in 2014, SWS in these cities has steadily increased, accompanied by a partial recovery of GWS, which was consistent with Lei et al. (2023) and L. Zhu et al. (2020). This change was primarily due to the augmented surface water supply, which has reduced reliance on groundwater extraction, particularly in urban areas with high domestic water consumption. In contrast, Hebei and Henan displayed similar patterns, with TWS changing slowly

and groundwater recovery remaining limited. This was due to the continuous dominance of agricultural water use. As shown in Figure 15, agricultural water consumption in both provinces consistently accounted for a higher proportion compared to other regions. Although ecological water use increased, heavy reliance on groundwater for irrigation offset potential recovery effects. Despite notable growth in SWS, high irrigation demands continued to deplete groundwater, constraining its recovery. Notably, SWS and GWS across all provinces reached historical highs in 2021. This was driven not only by water diversion from the MR-SNWDP but also by the impact of extreme precipitation events. That year, Henan experienced unprecedented heavy rainfall and flooding, including the catastrophic “July 20” rainstorm (Guo et al. 2023). The intense precipitation led to a rapid increase in SWS and replenished groundwater through infiltration. While the natural input temporarily masked the challenges of long-term groundwater recovery, it highlighted the complex influence of extreme climatic events on regional water dynamics. However, this surge primarily reflected short-term effects of rainfall, with limited contributions to lasting groundwater recovery, as the high proportion of agricultural water use remained a key constraint.

The annual variations in water use across the four regions are shown in Figure 15. Both domestic and ecological water use have increased significantly, highlighting that the MR-SNWDP has provided adequate water resources to support urban livelihoods and environmental restoration. One of the key goals of the project was to improve the ecological environment

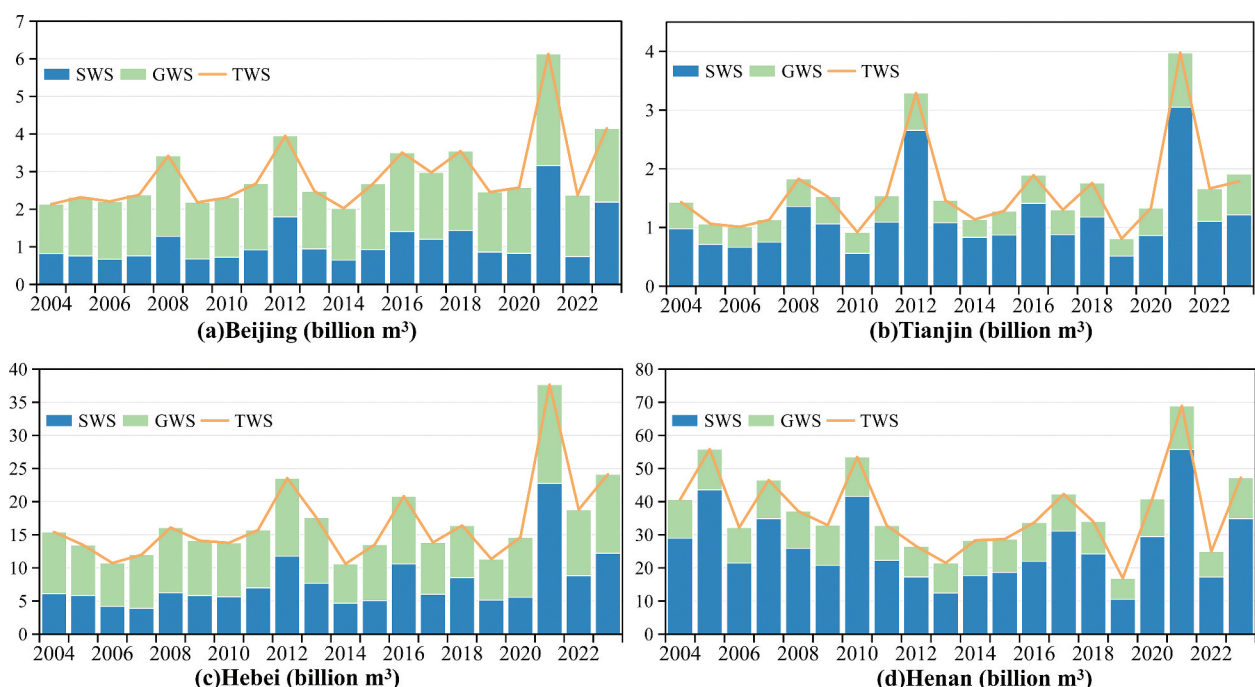


**Figure 14.** Annual variations in Surface Water Storage (SWS), Groundwater Storage (GWS) and Terrestrial Water Storage (TWS) in the WRA of the MR-SNWDP from 2004 to 2023.

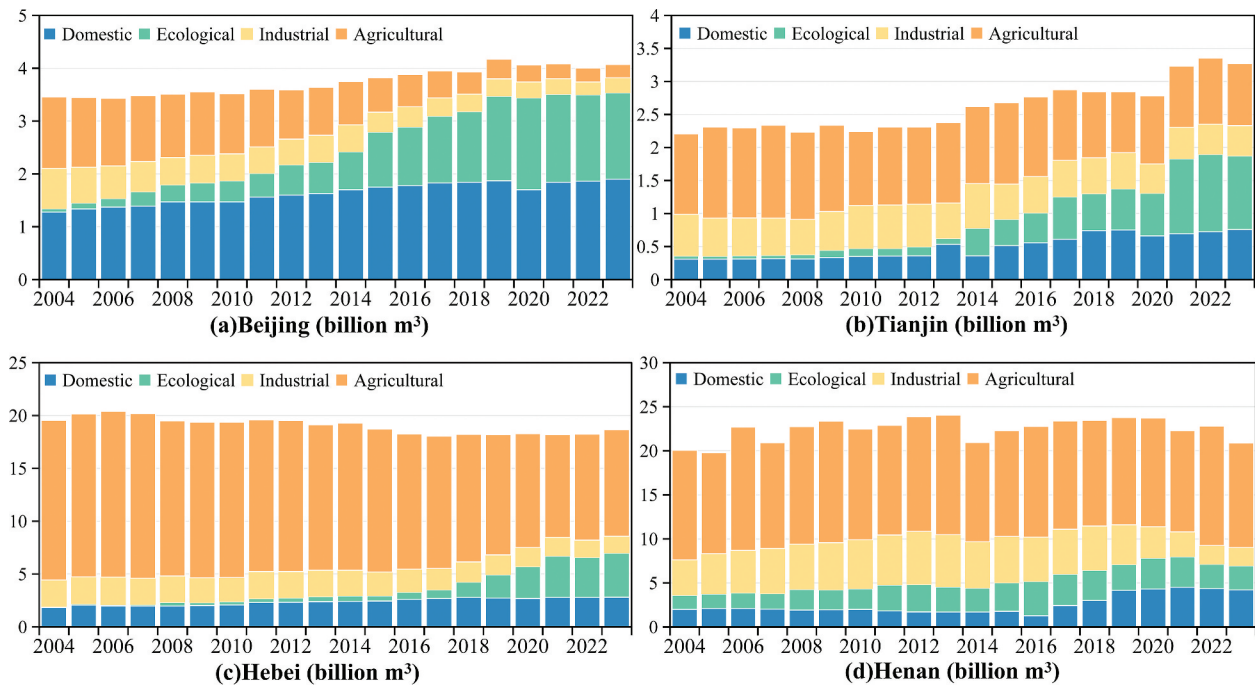


**Figure 15.** Annual variations in domestic, ecological, industrial and agricultural water use in the WRA of the MR-SNWDP from 2004 to 2023.

of northern China by increasing ecological water use to restore rivers, wetlands and lakes (Jiang 2015; Yan et al. 2023; C. Zhang et al. 2020). The proportion of ecological water use in total water consumption has steadily risen, particularly in Beijing and Tianjin after the opening of the project. This trend was closely linked to NDVI changes, reflecting higher vegetation coverage. This underscored the critical role of ecological water in supporting regional vegetation growth, especially in urban areas. Though ecological water use in Hebei and Henan has also increased, its impact on vegetation recovery has been more limited. The increase in NDVI in these provinces has been much slower compared to Beijing and Tianjin. This disparity was primarily due to the high proportion of agricultural water use and the slow groundwater replenishment caused by long-term over-exploitation, both of which have limited the effectiveness of ecological water use.

The MR-SNWDP has significantly altered the hydrological dynamics of the WRA, with the most noticeable impact on SWS. The project directly increased SWS through large-scale interregional water transfer, while GWS recovery occurred as an indirect effect. The replenishment of SWS reduced over-extraction of groundwater, contributing to some recovery in GWS levels, particularly in Beijing and Tianjin. This dynamic change highlighted how human intervention can enhance regional water sustainability by optimizing water resource allocation. However, the heavy reliance on agricultural water in Hebei and Henan not only weakened groundwater replenishment but also posed a long-term challenge

to regional hydrological balance. These findings offered valuable insights for future large-scale water diversion projects and the sustainable development of regional ecosystems.

#### 4.2. Integrated hydrological-ecological responses to the MR-SNWDP

The MR-SNWDP, as a large-scale interregional water diversion project, had far-reaching ecological impacts beyond the spatial reallocation of water resources. It significantly influenced vegetation dynamics and further modulated regional environmental conditions through the complex mechanisms, as illustrated in Figure 16.

The MR-SNWDP significantly modified the hydrological regime in the WRA, with a notable boost in surface water storage. Satellite-derived TWSA indicated a marked reversal in long-term hydrological patterns. Specifically, the annual rate of TWSA change transitioned from a declining trend of  $-1.874 \text{ cm/year}$  prior to 2014 to a rising trend of  $0.817 \text{ cm/year}$  following the operation. By 2023, both SWS and GWS in four provinces had risen to more than twice the respective baselines recorded in 2014 (Figure 14). Concurrently, ecological water consumption experienced a threefold increase, with the most significant gains observed in Beijing and Tianjin. This hydrological transformation was consistent with in-situ monitoring results. From 2014 to 2023, groundwater extraction across northern China declined by 47.2%, while deep and shallow aquifer levels in Hebei Province rose by 7.55 m and 3.01 m, respectively

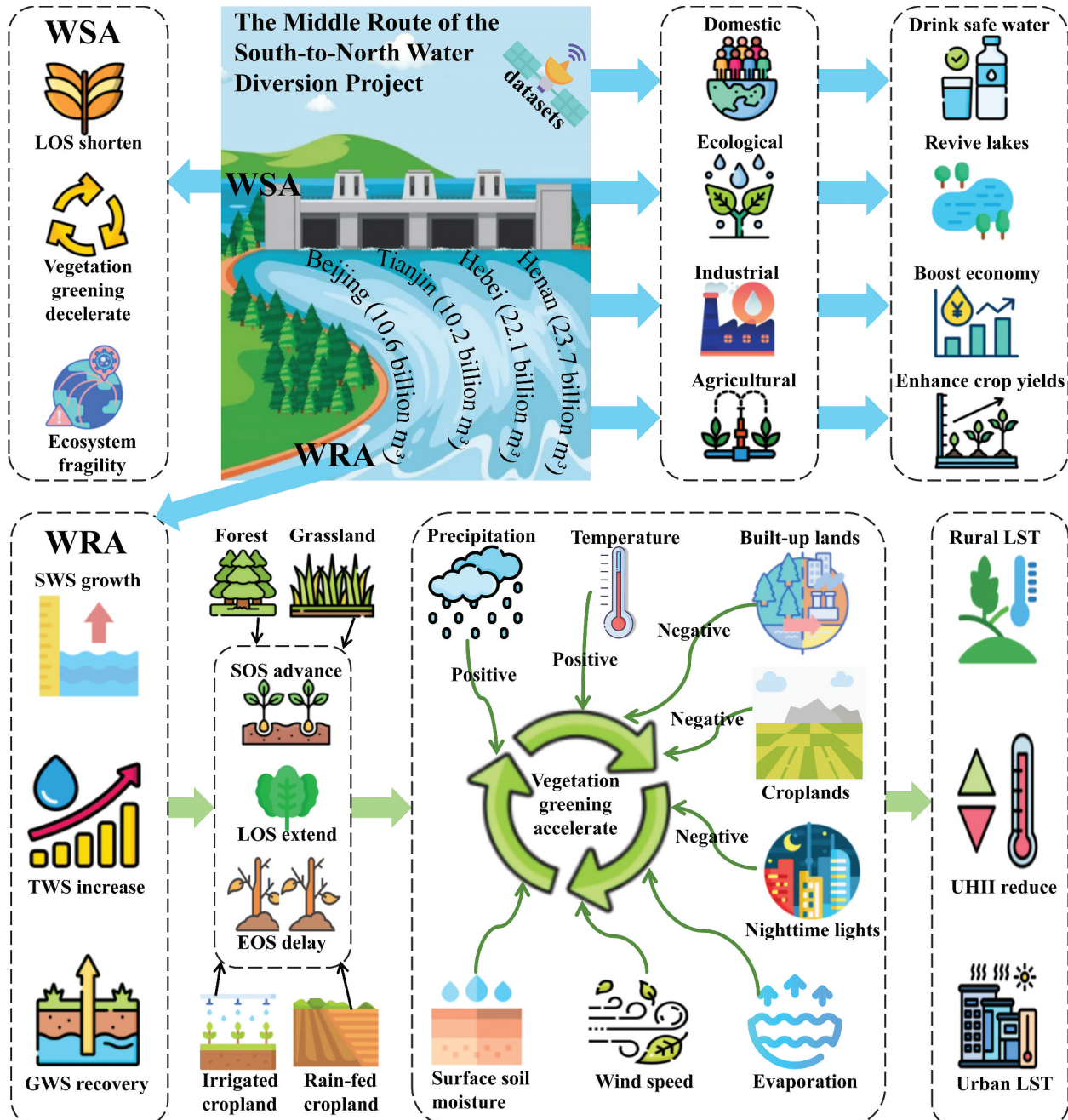


Figure 16. The schematic diagram of the impact mechanisms of the MR-SNWDP.

(Sheng, Zhang, and Yang 2024; C. Zhang et al. 2021). In Beijing, groundwater levels increased by an average of 2.9 m between 2014 and 2020 (Lei et al. 2023; Long et al. 2020). Due to the high quality of the transferred water, its function has shifted from being a supplementary source to becoming a primary supply for many cities. For instance, diverted water now accounts for 80% of the urban water supply in Beijing, 90% in Zhengzhou and nearly the entirety in Tianjin (Du et al. 2021; Lei et al. 2023). Ecological water transfers also played a pivotal role in large-scale environmental rehabilitation. By 2023, over 10 billion m<sup>3</sup> of diverted water was allocated to more than 50 rivers across northern China, substantially supporting aquatic ecosystem restoration (Y. Liu

et al. 2023; Shi et al. 2024). This reallocation enabled continuous flow in the Yongding River for four consecutive years, full hydrological connectivity in the Grand Canal for three years, and stable maintenance of ecological water levels in Baiyangdian Lake (Kattel et al. 2019; Wilson et al. 2017; Yan et al. 2023). These improvements stand in sharp contrast to the fragmented and desiccated river systems observed before the project was initiated (Sun et al. 2021; Zhai et al. 2022; R. Zhang et al. 2025). Collectively, the inter-basin transfer replaced excessive groundwater abstraction, enhanced wetland hydrology and facilitated regional biodiversity recovery in northern China.

The enhancement of regional water availability significantly promoted vegetation recovery across the

WRA. Following the initiation of the MR-SNWDP, the NDVI demonstrated a pronounced increase in positive trends, particularly in agricultural and ecological zones where supplementary irrigation improved water-use efficiency. This vegetation enhancement can be attributed to two principal aspects. First, increased water availability extended the growing season, as evidenced by the advanced sprouting and delayed senescence of plants, which was especially pronounced in irrigated croplands. As detailed in Section 3.2, this study is the first to quantitatively assess vegetation growing season changes at the regional scale induced by inter-basin water transfer. Second, the spatial heterogeneity in NDVI responses was shaped by the combined influences of climatic and anthropogenic factors. Attribution analysis (Section 3.3) revealed that PRE and TMP emerged as the primary positive drivers of NDVI growth, particularly in highly urbanized areas. Precipitation provided the necessary moisture for vegetation growth, while suitable temperatures enhanced photosynthesis and promoted biomass accumulation (Holdrege, Beard, and Kulmatiski 2021; Parton et al. 2012; Pitt and Heady 1978). These factors jointly contributed to sustained NDVI improvements, especially in years with significant precipitation increases, such as 2021. These results are consistent with previous studies. For instance, Xu, Yang, and Chen (2016) and G. Liu, Liu, and Yin (2013) demonstrated that favorable hydrothermal conditions substantially enhanced vegetation productivity in northern China. In contrast, the BUI was identified as a significant negative driver in major urban centers such as Beijing and Tianjin, where intensive domestic and industrial water demands constrained ecological water availability and vegetation recovery (Hu et al. 2023; Shahfahad, Talukdar, and Rahman 2024; K. Yang et al. 2021). Nevertheless, the MR-SNWDP partially alleviated part of this pressure by increasing baseline water supply, thereby maintaining vegetation resilience under high urban stress.

Vegetation restoration driven by the MR-SNWDP produced discernible impacts on urban thermal regimes across northern China. A statistically significant negative correlation was observed between NDVI and LST, corroborating prior findings that enhanced vegetation coverage mitigated surface temperatures through transpiration and shading effects (Peng et al. 2014; Weng, Lu, and Schubring 2004; Zhou, Zhang, Li, et al. 2016). These localized reductions in urban LST further alleviated the urban heat island effect (Buyantuyev and Wu 2010; X. Li et al. 2019). After 2014, the intensity of the UHI effect in Beijing exhibited a pronounced decline, while Hebei and Henan provinces experienced moderate reductions. In contrast, UHII in Tianjin showed a slight upward trend, which may be attributed to the comparatively limited expansion of urban greening and ecological infrastructure.

These spatial disparities underscored the heterogeneous influence of vegetation recovery on local thermal conditions, shaped by differences in urban planning strategies, green space distribution, and water resource accessibility (Jenerette et al. 2011; M. Li et al. 2025; Y. Li et al. 2024). While the NDVI-LST correlations have been widely studied, empirical evidence linking large-scale water diversion infrastructure to urban thermal mitigation remained scarce (Marzban, Sodoudi, and Preusker 2018; Peng et al. 2014; Weng, Lu, and Schubring 2004). This study contributed to filling this gap by providing regional-scale evidence that inter-basin water transfers can facilitate temperature regulation indirectly by supporting vegetation growth in densely populated urban agglomerations. The findings were consistent with recent studies indicating that improved hydrological conditions can enhance the effectiveness of urban ecology and local climate interventions, particularly in semi-arid and water-stressed regions (Fletcher et al. 2024; L. Zhu et al. 2015).

This study offered new evidence that large-scale inter-basin water transfers produced interlinked hydrological, ecological, and climatic effects across North China. The MR-SNWDP played a pivotal role in extending the vegetation growing season in the WRA by increasing SWS, a key component of TWS. This shift in water availability drove significant improvements in NDVI, which in turn regulated LST and contributed to the mitigation of UHII. This cascading mechanism underscored the central role of water resources redistribution in supporting ecosystem recovery and urban microclimate moderation in water-stressed regions. While earlier research often addressed these processes in isolation, this study integrated multi-source remote sensing datasets, including TWSA, NDVI and LST, to construct a comprehensive impact assessment framework, as shown in Figure 16. This system-based approach overcame the limitations of fragmented analyses and enabled a robust evaluation of eco-hydrological dynamics in response to engineered hydrological interventions. Furthermore, the study presented the first regional-scale quantification of growing season extension linked to improved water availability. The observed phenological changes, including earlier greening and delayed senescence, provided a vegetation-based explanation for the acceleration in NDVI trends. Additionally, the study revealed that water transfers indirectly moderated LST in urban centers, contributing to reductions in UHII. This dimension of climatic regulation had not been sufficiently addressed in prior literature, thus expanding the understanding of the broader environmental co-benefits of such infrastructure. The research also revealed regional disparities within the WRA, with climatic conditions and water use structures critically shaping the spatial patterns of vegetation dynamics and associated ecological benefits. Moreover, the study also

accounted for ecological consequences in the WSA. Although some areas demonstrated resilience, reductions in SWS and increased water exports led to slight reductions in vegetation growing season and greening trends, with ecosystems becoming more vulnerable to climate fluctuations and human activities in the WSA. In key WSA like Ankang in Shaanxi, efforts such as river-chief systems and ecological compensation have been implemented to protect water source ecosystems (K. Zhu et al. 2022). These findings suggested that the redistribution of water introduced ecological instability in the WSA, highlighting the need to reconcile water supply security with ecosystem sustainability.

## 5. Conclusions

This study systematically examined the hydrological, ecological, and climatic impacts of the MR-SNWDP from 2004 to 2023 on both the WSA and WRA. The results showed that the project significantly increased terrestrial water storage in the WRA, effectively alleviating groundwater overexploitation. Enhanced surface water availability facilitated earlier plant germination and delayed senescence, thereby extending the growing season and accelerating regional greening trends, particularly in areas where ecological water use accounted for a higher proportion. Changes in NDVI were primarily driven by positive contributions from climatic factors such as precipitation and temperature, while human activities exerted negative impacts. Improvements in vegetation coverage further played a critical role in mitigating urban heat island effect. In summary, the MR-SNWDP has made remarkable contributions to easing regional water scarcity, promoting vegetation recovery and regulating urban climates. However, in the long term, its effects on the ecological stability of the WSA warrant further attention, and future efforts should focus on balancing water resources redistribution with sustainable development to ensure the continuous benefits of the project.

## Disclosure statement

No potential conflict of interest was reported by the author(s).

## Funding

This work is supported by the National Key Research and Development Program of China [Grant number 2023YFC3209101], the National Natural Science Foundation of China program [Grants numbers 42461144214, 42371101], the Natural Science Foundation of Hubei Province [Grant number 2024AFB551], the CRSRI Open Research Program [Grant number CKWV20231198/KY], the Open Fund of National Engineering Research Center for Geographic Information System, China, University of Geosciences [Grant

number 2022KFJJ07], the Postdoctoral Fellowship Program and China Postdoctoral Science Foundation under [Grant Number BX20250027], and the numerical calculations in this paper have been done on the supercomputing system in the Supercomputing Center of Wuhan University.

## Notes on contributors

**Aoxue Cui** is a Master student in the State Key Laboratory of Information Engineering in Surveying, Mapping and Remote Sensing (LIESMARS), Wuhan University. Her research focuses on the spatiotemporal responses of vegetation growth to terrestrial water storage and the eco-hydrological impacts of the South-to-North Water Diversion Project.

**Chao Wang** is a professor at the State Key Laboratory of Information Engineering in Surveying, Mapping and Remote Sensing (LIESMARS), Wuhan University. His research interests include smart cities, land use change, and its ecological and environmental effects.

**Shuzhe Huang** received his PhD degree from the State Key Laboratory of Information Engineering in Surveying, Mapping and Remote Sensing (LIESMARS), Wuhan University. His research focuses on multi-source spatiotemporal data fusion and applications in drought disaster monitoring.

**Renke Ji** received her PhD degree from the State Key Laboratory of Information Engineering in Surveying, Mapping and Remote Sensing (LIESMARS), Wuhan University. Her research focuses on the attribution and prediction of spatiotemporal characteristics and imbalances in terrestrial water storage.

**Mingming Jia** is a professor at the Northeast Institute of Geography and Agroecology, Chinese Academy of Sciences. Her research focuses on remote sensing of coastal ecological environments.

**Xiang Zhang** is a professor at China University of Geosciences (Wuhan). His research interests include drought remote sensing observation and intelligent disaster mitigation services.

**Wei Wang** is a professor at the State Key Laboratory of Information Engineering in Surveying, Mapping and Remote Sensing (LIESMARS), Wuhan University. His research focuses on spatial information systems and smart city applications.

**Nengcheng Chen** is a professor at China University of Geosciences (Wuhan). His research interests include spatiotemporal digital twins, geospatial sensor networks, and smart watershed management.

## ORCID

Aoxue Cui  <http://orcid.org/0009-0006-1303-261X>

## Data availability statement

The data that support the findings of this study are available from the corresponding author upon reasonable request.

## References

- Badeck, F. W., A. Bondeau, K. Böttcher, D. Doktor, W. Lucht, J. Schaber, and S. Sitch. 2004. "Responses of Spring Phenology to Climate Change." *New Phytologist* 162 (2): 295–309. <https://doi.org/10.1111/j.1469-8137.2004.01059.x>.
- Boretti, A., and L. Rosa. 2019. "Reassessing the Projections of the World Water Development Report." *NPJ Clean Water* 2 (1): 15. <https://doi.org/10.1038/s41545-019-0039-9>.
- Brunsdon, C., A. S. Fotheringham, and M. E. Charlton. 1996. "Geographically Weighted Regression: A Method for Exploring Spatial Nonstationarity." *Geographical Analysis* 28 (4): 281–298. <https://doi.org/10.1111/j.1538-4632.1996.tb00936.x>.
- Buyantuyev, A., and J. Wu. 2010. "Urban Heat Islands and Landscape Heterogeneity: Linking Spatiotemporal Variations in Surface Temperatures to Land-Cover and Socioeconomic Patterns." *Landscape Ecology* 25 (1): 17–33. <https://doi.org/10.1007/s10980-009-9402-4>.
- Clinton, N., and P. Gong. 2013. "MODIS Detected Surface Urban Heat Islands and Sinks: Global Locations and Controls." *Remote Sensing of Environment* 134:294–304. <https://doi.org/10.1016/j.rse.2013.03.008>.
- Cosgrove, W. J., and D. P. Loucks. 2015. "Water Management: Current and Future Challenges and Research Directions." *Water Resources Research* 51 (6): 4823–4839. <https://doi.org/10.1002/2014WR016869>.
- Das, D. K. 2019. "Climate Change and Interlinking of Indian Rivers: Lessons from Canadian Inter-Basin Water Transfer Experiences." *Nation-Building, Education and Culture in India and Canada*: 111–133. [https://doi.org/10.1007/978-981-13-6741-0\\_8](https://doi.org/10.1007/978-981-13-6741-0_8).
- Ditmar, P. 2018. "Conversion of Time-Varying Stokes Coefficients into Mass Anomalies at the Earth's Surface Considering the Earth's Oblateness." *Journal of Geodesy* 92 (12): 1401–1412. <https://doi.org/10.1007/s00190-018-1128-0>.
- Du, Z., L. Ge, A. H.-M. Ng, X. Lian, Q. Zhu, F. G. Horgan, and Q. Zhang. 2021. "Analysis of the Impact of the South-to-North Water Diversion Project on Water Balance and Land Subsidence in Beijing, China Between 2007 and 2020." *Journal of Hydrology* 603:126990. <https://doi.org/10.1016/j.jhydrol.2021.126990>.
- Elvidge, C. D., K. Baugh, M. Zhizhin, F. C. Hsu, and T. Ghosh. 2017. "VIIRS Night-Time Lights." *International Journal of Remote Sensing* 38 (21): 5860–5879. <https://doi.org/10.1080/01431161.2017.1342050>.
- Fan, L., H. Wang, W. Lai, and C. Wang. 2015. "Administration of Water Resources in Beijing: Problems and Countermeasures." *Water Policy* 17 (4): 563–580. <https://doi.org/10.2166/wp.2014.407>.
- Fang, Q., L. Ma, T. Green, Q. Yu, T. Wang, and L. Ahuja. 2010. "Water Resources and Water Use Efficiency in the North China Plain: Current Status and Agronomic Management Options." *Agricultural Water Management* 97 (8): 1102–1116. <https://doi.org/10.1016/j.agwat.2010.01.008>.
- Filippa, G., E. Cremonese, M. Migliavacca, M. Galvagno, M. Forkel, L. Wingate, E. Tomelleri, U. M. Di Cellà, and A. D. Richardson. 2016. "Phenopix: AR Package for Image-Based Vegetation Phenology." *Agricultural and Forest Meteorology* 220:141–150. <https://doi.org/10.1016/j.agrformet.2016.01.006>.
- Fletcher, T. D., M. J. Burns, K. L. Russell, P. Hamel, S. Duchesne, F. Cherqui, and A. H. Roy. 2024. "Concepts and Evolution of Urban Hydrology." *Nature Reviews Earth & Environment* 5 (11): 1–13. <https://doi.org/10.1038/s43017-024-00599-x>.
- Foster, S., H. Garduno, R. Evans, D. Olson, Y. Tian, W. Zhang, and Z. Han. 2004. "Quaternary Aquifer of the North China Plain—Assessing and Achieving Groundwater Resource Sustainability." *Hydrogeology Journal* 12 (1): 81–93. <https://doi.org/10.1007/s10040-003-0300-6>.
- Fotheringham, A. S., C. Brunsdon, and M. Charlton. 2009. "Geographically Weighted Regression." *The SAGE Handbook of Spatial Analysis* 1:243–254. <https://doi.org/10.4135/9780857020130.n13>.
- Friedl, M. A., D. Sulla-Menashe, B. Tan, A. Schneider, N. Ramankutty, A. Sibley, and X. Huang. 2010. "MODIS Collection 5 Global Land Cover: Algorithm Refinements and Characterization of New Datasets." *Remote Sensing of Environment* 114 (1): 168–182. <https://doi.org/10.1016/j.rse.2009.08.016>.
- Gleick, P. H. 2003. "Global Freshwater Resources: Soft-Path Solutions for the 21st Century." *Science* 302 (5650): 1524–1528. <https://doi.org/10.1126/science.1089967>.
- Green, P. A., C. J. Vörösmarty, I. Harrison, T. Farrell, L. Sáenz, and B. M. Fekete. 2015. "Freshwater Ecosystem Services Supporting Humans: Pivoting from Water Crisis to Water Solutions." *Global Environmental Change* 34:108–118. <https://doi.org/10.1016/j.gloenvcha.2015.06.007>.
- Grigg, N. S. 2023. "Large-Scale Water Development in the United States: TVA and the California State Water Project." *International Journal of Water Resources Development* 39 (1): 70–88. <https://doi.org/10.1080/07900627.2021.1969224>.
- Gu, W., D. Shao, and Y. Jiang. 2012. "Risk Evaluation of Water Shortage in Source Area of Middle Route Project for South-to-North Water Transfer in China." *Water Resources Management* 26 (12): 3479–3493. <https://doi.org/10.1007/s11269-012-0086-1>.
- Guo, X., J. Cheng, C. Yin, Q. Li, R. Chen, and J. Fang. 2023. "The Extraordinary Zhengzhou Flood of 7/20, 2021: How Extreme Weather and Human Response Compounding to the Disaster." *Cities* 134:104168. <https://doi.org/10.1016/j.cities.2022.104168>.
- Hersbach, H., B. Bell, P. Berrisford, S. Hirahara, A. Horányi, J. Muñoz-Sabater, J. Nicolas, C. Peubey, R. Radu, and D. Schepers. 2020. "The ERA5 Global Reanalysis." *Quarterly Journal of the Royal Meteorological Society* 146 (730): 1999–2049. <https://doi.org/10.1002/qj.3803>.
- Holben, B. N. 1986. "Characteristics of Maximum-Value Composite Images from Temporal AVHRR Data." *International Journal of Remote Sensing* 7 (11): 1417–1434. <https://doi.org/10.1080/01431168608948945>.
- Holdrege, M. C., K. H. Beard, and A. Kulmatiski. 2021. "Woody Plant Growth Increases with Precipitation Intensity in a Cold Semiarid System." *Ecology* 102 (1): e03212. <https://doi.org/10.1002/ecy.3212>.
- Hu, T., J. Dong, S. Qiu, Z. Yang, Y. Zhao, X. Cheng, and J. Peng. 2023. "Stage Response of Vegetation Dynamics to Urbanization in Megacities: A Case Study of Changsha City, China." *Science of the Total Environment* 858 (Pt 3): 159659. <https://doi.org/10.1016/j.scitotenv.2022.159659>.
- Huete, A., K. Didan, T. Miura, E. P. Rodriguez, X. Gao, and L. G. Ferreira. 2002. "Overview of the Radiometric and Biophysical Performance of the MODIS Vegetation

- Indices." *Remote Sensing of Environment* 83 (1–2): 195–213. [https://doi.org/10.1016/S0034-4257\(02\)00096-2](https://doi.org/10.1016/S0034-4257(02)00096-2).
- Jackson, R. B., S. R. Carpenter, C. N. Dahm, D. M. McKnight, R. J. Naiman, S. L. Postel, and S. W. Running. 2001. "Water in a Changing World." *Ecological Applications* 11 (4): 1027–1045. [https://doi.org/10.1890/1051-0761\(2001\)011\[1027:WIACW\]2.0.CO;2](https://doi.org/10.1890/1051-0761(2001)011[1027:WIACW]2.0.CO;2).
- Jenerette, G. D., S. L. Harlan, W. L. Stefanov, and C. A. Martin. 2011. "Ecosystem Services and Urban Heat Riskscape Moderation: Water, Green Spaces, and Social Inequality in Phoenix, USA." *Ecological Applications* 21 (7): 2637–2651. <https://doi.org/10.1890/10-1493.1>.
- Jeong, S. J., C. H. Ho, H. J. Gim, and M. E. Brown. 2011. "Phenology Shifts at Start vs. End of Growing Season in Temperate Vegetation Over the Northern Hemisphere for the Period 1982–2008." *Global Change Biology* 17 (7): 2385–2399. <https://doi.org/10.1111/j.1365-2486.2011.02397.x>.
- Jia, J. 2016. "A Technical Review of Hydro-Project Development in China." *Engineering* 2 (3): 302–312. <https://doi.org/10.1016/J.ENG.2016.03.008>.
- Jiang, Y. 2009. "China's Water Scarcity." *Journal of Environmental Management* 90 (11): 3185–3196. <https://doi.org/10.1016/j.jenvman.2009.04.016>.
- Jiang, Y. 2015. "China's Water Security: Current Status, Emerging Challenges and Future Prospects." *Environmental Science & Policy* 54:106–125. <https://doi.org/10.1016/j.envsci.2015.06.006>.
- Jonsson, P., and L. Eklundh. 2002. "Seasonality Extraction by Function Fitting to Time-Series of Satellite Sensor Data." *IEEE Transactions on Geoscience and Remote Sensing* 40 (8): 1824–1832. <https://doi.org/10.1109/TGRS.2002.802519>.
- Kattel, G. R., W. Shang, Z. Wang, and J. Langford. 2019. "China's South-to-North Water Diversion Project Empowers Sustainable Water Resources System in the North." *Sustainability* 11 (13): 3735. <https://doi.org/10.3390-su11133735>.
- Kim, H. H. 1992. "Urban Heat Island." *International Journal of Remote Sensing* 13 (12): 2319–2336. <https://doi.org/10.1080/01431169208904271>.
- Kong, D., T. R. McVicar, M. Xiao, Y. Zhang, J. L. Peña-Arancibia, G. Filippa, Y. Xie, and X. Gu. 2022. "Phenofit: An R Package for Extracting Vegetation Phenology from Time Series Remote Sensing." *Methods in Ecology and Evolution* 13 (7): 1508–1527. <https://doi.org/10.1111/2041-210X.13870>.
- Kuang, W. 2019. "Mapping Global Impervious Surface Area and Green Space Within Urban Environments." *Science China Earth Sciences* 62 (10): 1591–1606. <https://doi.org/10.1007/s11430-018-9342-3>.
- Lei, K., F. Ma, B. Chen, Y. Luo, W. Cui, L. Zhao, X. Wang, and A. Sun. 2023. "Effects of South-to-North Water Diversion Project on Groundwater and Land Subsidence in Beijing, China." *Bulletin of Engineering Geology and the Environment* 82 (1): 18. <https://doi.org/10.1007/s10064-022-03021-2>.
- Li, L., L. Zhang, J. Xia, C. J. Gippel, R. Wang, and S. Zeng. 2015. "Implications of Modelled Climate and Land Cover Changes on Runoff in the Middle Route of the South to North Water Transfer Project in China." *Water Resources Management* 29 (8): 2563–2579. <https://doi.org/10.1007/s11269-015-0957-3>.
- Li, M., C. Wang, Y. Wu, M. Santamouris, and S. Lu. 2025. "Assessing Spatial Inequities of Thermal Environment and Blue-Green Intervention for Vulnerable Populations in Dense Urban Areas." *Urban Climate* 59:102328. <https://doi.org/10.1016/j.uclim.2025.102328>.
- Li, S., J. Li, and Q. Zhang. 2011. "Water Quality Assessment in the Rivers Along the Water Conveyance System of the Middle Route of the South to North Water Transfer Project (China) Using Multivariate Statistical Techniques and Receptor Modeling." *Journal of Hazardous Materials* 195:306–317. <https://doi.org/10.1016/j.jhazmat.2011.08.043>.
- Li, X., and Y. Zhou. 2017. "Urban Mapping Using DMSP/OLS Stable Night-Time Light: A Review." *International Journal of Remote Sensing* 38 (21): 6030–6046. <https://doi.org/10.1080/01431161.2016.1274451>.
- Li, X., Y. Zhou, S. Yu, G. Jia, H. Li, and W. Li. 2019. "Urban Heat Island Impacts on Building Energy Consumption: A Review of Approaches and Findings." *Energy* 174:407–419. <https://doi.org/10.1016/j.energy.2019.02.183>.
- Li, X., L. Zou, J. Xia, L. Zhang, F. Wang, and M. Li. 2024. "Response of Blue-Green Water to Climate and Vegetation Changes in the Water Source Region of China's South-North Water Diversion Project." *Journal of Hydrology* 634:131061. <https://doi.org/10.1016/j.jhydrol.2024.131061>.
- Li, Y., J.-C. Svenning, W. Zhou, K. Zhu, J. F. Abrams, T. M. Lenton, W. J. Ripple, Z. Yu, S. N. Teng, and R. R. Dunn. 2024. "Green Spaces Provide Substantial but Unequal Urban Cooling Globally." *Nature Communications* 15 (1): 7108. <https://doi.org/10.1038/s41467-024-51355-0>.
- Liu, C., J. Yu, and E. Kendy. 2001. "Groundwater Exploitation and its Impact on the Environment in the North China Plain." *Water International* 26 (2): 265–272. <https://doi.org/10.1080/02508060108686913>.
- Liu, G., H. Liu, and Y. Yin. 2013. "Global Patterns of NDVI-Indicated Vegetation Extremes and Their Sensitivity to Climate Extremes." *Environmental Research Letters* 8 (2): 025009. <https://doi.org/10.1088/1748-9326/8/2/025009>.
- Liu, Y., Z. Xin, S. Sun, C. Zhang, and G. Fu. 2023. "Assessing Environmental, Economic, and Social Impacts of Inter-Basin Water Transfer in China." *Journal of Hydrology* 625:130008. <https://doi.org/10.1016/j.jhydrol.2023.130008>.
- Long, D., W. Yang, B. R. Scanlon, J. Zhao, D. Liu, P. Burek, Y. Pan, L. You, and Y. Wada. 2020. "South-to-North Water Diversion Stabilizing Beijing's Groundwater Levels." *Nature Communications* 11 (1): 3665. <https://doi.org/10.1038/s41467-020-17428-6>.
- Lyu, H.-M., Y.-S. Xu, W.-C. Cheng, and A. Arulrajah. 2018. "Flooding Hazards Across Southern China and Prospective Sustainability Measures." *Sustainability* 10 (5): 1682. <https://doi.org/10.3390/su10051682>.
- Mann, H. B. 1945. "Nonparametric Tests Against Trend." *Econometrica: Journal of the Econometric Society* 13 (3): 245–259. <https://doi.org/10.2307/1907187>.
- Marzban, F., S. Sodoudi, and R. Preusker. 2018. "The Influence of Land-Cover Type on the Relationship Between NDVI-LST and LST-T Air." *International Journal of Remote Sensing* 39 (5): 1377–1398. <https://doi.org/10.1080/01431161.2017.1402386>.
- Mekonnen, M. M., and A. Y. Hoekstra. 2016. "Four Billion People Facing Severe Water Scarcity." *Science Advances* 2 (2): e1500323. <https://doi.org/10.1126/sciadv.1500323>.
- Parton, W., J. Morgan, D. Smith, S. Del Grosso, L. Prihodko, D. LeCain, R. Kelly, and S. Lutz. 2012. "Impact of Precipitation Dynamics on Net Ecosystem

- Productivity." *Global Change Biology* 18 (3): 915–927. <https://doi.org/10.1111/j.1365-2486.2011.02611.x>.
- Peng, S.-S., S. Piao, Z. Zeng, P. Ciais, L. Zhou, L. Z. Li, R. B. Myneni, Y. Yin, and H. Zeng. 2014. "Afforestation in China Cools Local Land Surface Temperature." *Proceedings of the National Academy of Sciences* 111 (8): 2915–2919. <https://doi.org/10.1073/pnas.1315126111>.
- Piao, S., P. Ciais, Y. Huang, Z. Shen, S. Peng, J. Li, L. Zhou, H. Liu, Y. Ma, and Y. Ding. 2010. "The Impacts of Climate Change on Water Resources and Agriculture in China." *Nature* 467 (7311): 43–51. <https://doi.org/10.1038/nature09364>.
- Pitt, M., and H. Heady. 1978. "Responses of Annual Vegetation to Temperature and Rainfall Patterns in Northern California." *Ecology* 59 (2): 336–350. <https://doi.org/10.2307/1936378>.
- Reed, B. C., J. F. Brown, D. VanderZee, T. R. Loveland, J. W. Merchant, and D. O. Ohlen. 1994. "Measuring Phenological Variability from Satellite Imagery." *Journal of Vegetation Science* 5 (5): 703–714. <https://doi.org/10.2307/3235884>.
- Richardson, A. D., T. F. Keenan, M. Migliavacca, Y. Ryu, O. Sonnentag, and M. Toomey. 2013. "Climate Change, Phenology, and Phenological Control of Vegetation Feedbacks to the Climate System." *Agricultural and Forest Meteorology* 169:156–173. <https://doi.org/10.1016/j.agrformet.2012.09.012>.
- Rodell, M., P. Houser, U. Jambor, J. Gottschalck, K. Mitchell, C.-J. Meng, K. Arsenault, B. Cosgrove, J. Radakovich, and M. Bosilovich. 2004. "The Global Land Data Assimilation System." *Bulletin of the American Meteorological Society* 85 (3): 381–394. <https://doi.org/10.1175/BAMS-85-3-381>.
- Scanlon, B. R., B. L. Ruddell, P. M. Reed, R. I. Hook, C. Zheng, V. C. Tidwell, and S. Siebert. 2017. "The Food-Energy-Water Nexus: Transforming Science for Society." *Water Resources Research* 53 (5): 3550–3556. <https://doi.org/10.1002/2017WR020889>.
- Sen, P. K. 1968. "Estimates of the Regression Coefficient Based on Kendall's Tau." *Journal of the American Statistical Association* 63 (324): 1379–1389. <https://doi.org/10.1080/01621459.1968.10480934>.
- Shahfahad, S., M. W. N. Talukdar, and A. Rahman. 2024. "Urban Expansion and Vegetation Dynamics: The Role of Protected Areas in Preventing Vegetation Loss in a Growing Mega City." *Habitat International* 150:103129. <https://doi.org/10.1016/j.habitatint.2024.103129>.
- Sheng, J., R. Zhang, and H. Yang. 2024. "Inter-Basin Water Transfers and Water Rebound Effects: The South-North Water Transfer Project in China." *Journal of Hydrology* 638:131516. <https://doi.org/10.1016/j.jhydrol.2024.131516>.
- Shi, M., M. Gao, Z. Chen, M. Lyu, H. Gong, Y. Zhai, and Y. Pan. 2024. "Land Subsidence in Beijing: Response to the Joint Influence of the South-to-North Water Diversion Project and Ecological Water Replenishment, Observed by Satellite Radar Interferometry." *GIScience & Remote Sensing* 61 (1): 2315708. <https://doi.org/10.1080/15481603.2024.2315708>.
- Sun, S., X. Zhou, H. Liu, Y. Jiang, H. Zhou, C. Zhang, and G. Fu. 2021. "Unraveling the Effect of Inter-Basin Water Transfer on Reducing Water Scarcity and Its Inequality in China." *Water Research* 194:116931. <https://doi.org/10.1016/j.watres.2021.116931>.
- Tarek, M., F. P. Brissette, and R. Arsenault. 2020. "Evaluation of the ERA5 Reanalysis as a Potential Reference Dataset for Hydrological Modelling Over North America." *Hydrology and Earth System Sciences* 24 (5): 2527–2544. <https://doi.org/10.5194/hess-24-2527-2020>.
- Vörösmarty, C. J., P. B. McIntyre, M. O. Gessner, D. Dudgeon, A. Prusevich, P. Green, S. Glidden, S. E. Bunn, C. A. Sullivan, and C. R. Liermann. 2010. "Global Threats to Human Water Security and River Biodiversity." *Nature* 467 (7315): 555–561. <https://doi.org/10.1038/nature09440>.
- Wan, Z. 2008. "New Refinements and Validation of the MODIS Land-Surface Temperature/Emissivity Products." *Remote Sensing of Environment* 112 (1): 59–74. <https://doi.org/10.1016/j.rse.2006.06.026>.
- Wang, C., A. Cui, R. Ji, S. Huang, P. Li, N. Chen, and Z. Shao. 2025. "Spatiotemporal Responses of Global Vegetation Growth to Terrestrial Water Storage." *Remote Sensing* 17 (10): 1701. <https://doi.org/10.3390/rs17101701>.
- Wang, C., L. Ma, Y. Zhang, N. Chen, and W. Wang. 2022. "Spatiotemporal Dynamics of Wetlands and Their Driving Factors Based on PLS-SEM: A Case Study in Wuhan." *Science of the Total Environment* 806:151310. <https://doi.org/10.1016/j.scitotenv.2021.151310>.
- Wang, S., Y. Liu, J. Guo, J. Liu, and H. Chai. 2024. "Impacts of the Middle Route of the South-to-North Water Diversion Project on Land Surface Temperature and Fractional Vegetation Coverage in the Danjiang River Basin." *Remote Sensing* 16 (14): 2665. <https://doi.org/10.3390/rs16142665>.
- Wang, Y., C. Wang, C. Zhang, J. Liang, W. Mi, G. Song, Y. Zhu, S. Wang, Y. Shang, and Y. Bi. 2023. "Water Quality Variation in the Middle Route of South-to-North Water Diversion Project, China." *Frontiers in Environmental Science* 11:945884. <https://doi.org/10.3389/fenvs.2023.945884>.
- Webber, M., B. Crow-Miller, and S. Rogers. 2017. "The South–North Water Transfer Project: Remaking the Geography of China." *Regional Studies* 51 (3): 370–382. <https://doi.org/10.1080/00343404.2016.1265647>.
- Wei, S., H. Yang, K. Abbaspour, J. Mousavi, and A. Gnauck. 2010. "Game Theory Based Models to Analyze Water Conflicts in the Middle Route of the South-to-North Water Transfer Project in China." *Water Research* 44 (8): 2499–2516. <https://doi.org/10.1016/j.watres.2010.01.021>.
- Weng, Q., D. Lu, and J. Schubring. 2004. "Estimation of Land Surface Temperature–Vegetation Abundance Relationship for Urban Heat Island Studies." *Remote Sensing of Environment* 89 (4): 467–483. <https://doi.org/10.1016/j.rse.2003.11.005>.
- White, M. A., K. M. de Beurs, K. Didan, D. W. Inouye, A. D. Richardson, O. P. Jensen, J. O'keefe, G. Zhang, R. R. Nemani, and W. J. van Leeuwen. 2009. "Intercomparison, Interpretation, and Assessment of Spring Phenology in North America Estimated from Remote Sensing for 1982–2006." *Global Change Biology* 15 (10): 2335–2359. <https://doi.org/10.1111/j.1365-2486.2009.01910.x>.
- Wilson, M. C., X.-Y. Li, Y.-J. Ma, A. T. Smith, and J. Wu. 2017. "A Review of the Economic, Social, and Environmental Impacts of China's South–North Water Transfer Project: A Sustainability Perspective." *Sustainability* 9 (8): 1489. <https://doi.org/10.3390/su9081489>.
- Xu, Y., J. Yang, and Y. Chen. 2016. "NDVI-Based Vegetation Responses to Climate Change in an Arid

- Area of China." *Theoretical and Applied Climatology* 126:213–222. <https://doi.org/10.1007/s00704-015-1572-1>.
- Yan, H., Y. Lin, Q. Chen, J. Zhang, S. He, T. Feng, Z. Wang, C. Chen, and J. Ding. 2023. "A Review of the Eco-Environmental Impacts of the South-to-North Water Diversion: Implications for Interbasin Water Transfers." *Engineering* 30:161–169. <https://doi.org/10.1016/j.eng.2023.05.012>.
- Yang, K., W. Sun, Y. Luo, and L. Zhao. 2021. "Impact of Urban Expansion on Vegetation: The Case of China (-2000–2018)." *Journal of Environmental Management* 291:112598. <https://doi.org/10.1016/j.jenvman.2021.112598>.
- Yang, L., F. Qian, D.-X. Song, and K.-J. Zheng. 2016. "Research on Urban Heat-Island Effect." *Procedia Engineering* 169:11–18. <https://doi.org/10.1016/j.proeng.2016.10.002>.
- Yi, S., and N. Sneeuw. 2021. "Filling the Data Gaps within GRACE Missions Using Singular Spectrum Analysis." *Journal of Geophysical Research: Solid Earth* 126 (5): e2020JB021227. <https://doi.org/10.1029/2020JB021227>.
- Zeng, L., B. D. Wardlow, D. Xiang, S. Hu, and D. Li. 2020. "A Review of Vegetation Phenological Metrics Extraction Using Time-Series, Multispectral Satellite Data." *Remote Sensing of Environment* 237:111511. <https://doi.org/10.1016/j.rse.2019.111511>.
- Zhai, L., S. Cheng, H. Sang, W. Xie, L. Gan, and T. Wang. 2022. "Remote Sensing Evaluation of Ecological Restoration Engineering Effect: A Case Study of the Yongding River Watershed, China." *Ecological Engineering* 182:106724. <https://doi.org/10.1016/j.ecoleng.2022.106724>.
- Zhang, C., Q. Duan, P. J. F. Yeh, Y. Pan, H. Gong, W. Gong, Z. Di, X. Lei, W. Liao, and Z. Huang. 2020. "The Effectiveness of the South-to-North Water Diversion Middle Route Project on Water Delivery and Groundwater Recovery in North China Plain." *Water Resources Research* 56 (10): e2019WR026759. <https://doi.org/10.1029/2019WR026759>.
- Zhang, C., Q. Duan, P. J.-F. Yeh, Y. Pan, H. Gong, H. Moradkhani, W. Gong, X. Lei, W. Liao, and L. Xu. 2021. "Sub-regional Groundwater Storage Recovery in North China Plain After the South-to-North Water Diversion Project." *Journal of Hydrology* 597:126156. <https://doi.org/10.1016/j.jhydrol.2021.126156>.
- Zhang, J., Y. Zhang, G. Sun, C. Song, M. P. Dannenberg, J. Li, N. Liu, K. Zhang, Q. Zhang, and L. Hao. 2021. "Vegetation Greening Weakened the Capacity of Water Supply to China's South-to-North Water Diversion Project." *Hydrology and Earth System Sciences* 25 (10): 5623–5640. <https://doi.org/10.5194/hess-25-5623-2021>.
- Zhang, Q. 2009. "The South-to-North Water Transfer Project of China: Environmental Implications and Monitoring Strategy 1." *JAWRA Journal of the American Water Resources Association* 45 (5): 1238–1247. <https://doi.org/10.1111/j.1752-1688.2009.00357.x>.
- Zhang, Q., X. Gu, V. P. Singh, P. Shi, and M. Luo. 2017. "Timing of Floods in Southeastern China: Seasonal Properties and Potential Causes." *Journal of Hydrology* 552:732–744. <https://doi.org/10.1016/j.jhydrol.2017.07.039>.
- Zhang, Q., Z. Xu, Z. Shen, S. Li, and S. Wang. 2009. "The Han River Watershed Management Initiative for the South-to-North Water Transfer Project (Middle Route) of China." *Environmental Monitoring and Assessment* 148 (1–4): 369–377. <https://doi.org/10.1007/s10661-008-0167-z>.
- Zhang, R., T. Wang, G. Liu, A. Shama, A. Liu, X. Wang, L. Deng, and W. Mao. 2025. "Ground Subsidence Evolution and Groundwater Variation in the Middle Route of South to North Water Diversion Project." *Scientific Reports* 15 (1): 1–21. <https://doi.org/10.1038/s41598-025-04307-7>.
- Zhang, X., M. A. Friedl, C. B. Schaaf, A. H. Strahler, J. C. Hodges, F. Gao, B. C. Reed, and A. Huete. 2003. "Monitoring Vegetation Phenology Using MODIS." *Remote Sensing of Environment* 84 (3): 471–475. [https://doi.org/10.1016/S0034-4257\(02\)00135-9](https://doi.org/10.1016/S0034-4257(02)00135-9).
- Zhou, D., L. Zhang, L. Hao, G. Sun, Y. Liu, and C. Zhu. 2016. "Spatiotemporal Trends of Urban Heat Island Effect Along the Urban Development Intensity Gradient in China." *Science of the Total Environment* 544:617–626. <https://doi.org/10.1016/j.scitotenv.2015.11.168>.
- Zhou, D., L. Zhang, D. Li, D. Huang, and C. Zhu. 2016. "Climate-Vegetation Control on the Diurnal and Seasonal Variations of Surface Urban Heat Islands in China." *Environmental Research Letters* 11 (7): 074009. <https://doi.org/10.1088/1748-9326/11/7/074009>.
- Zhu, K., Y. Zhang, M. Wang, and H. Liu. 2022. "The Ecological Compensation Mechanism in a Cross-Regional Water Diversion Project Using Evolutionary Game Theory: The Case of the Hanjiang River Basin, China." *Water* 14 (7): 1151. <https://doi.org/10.3390/w14071151>.
- Zhu, L., H. Gong, Y. Chen, S. Wang, Y. Ke, G. Guo, X. Li, B. Chen, H. Wang, and P. Teatini. 2020. "Effects of Water Diversion Project on Groundwater System and Land Subsidence in Beijing, China." *Engineering Geology* 276:105763. <https://doi.org/10.1016/j.enggeo.2020.105763>.
- Zhu, L., H. Gong, Z. Dai, T. Xu, and X. Su. 2015. "An Integrated Assessment of the Impact of Precipitation and Groundwater on Vegetation Growth in Arid and Semiarid Areas." *Environmental Earth Sciences* 74 (6): 5009–5021. <https://doi.org/10.1007/s12665-015-4513-5>.
- Zou, J., C. Zhan, Z. Xie, P. Qin, and S. Jiang. 2016. "Climatic Impacts of the Middle Route of the South-to-North Water Transfer Project Over the Haihe River Basin in North China Simulated by a Regional Climate Model." *Journal of Geophysical Research: Atmospheres* 121 (15): 8983–8999. <https://doi.org/10.1002/2016JD024997>.

## Appendix

**Table A1.** Global Moran's I Index of NDVI for 2004, 2014, and 2023.

Year	Moran's I	Z-Value	P-Value
2004	0.898***	35.902	< 0.001
2014	0.901***	36.028	< 0.001
2023	0.915***	36.739	< 0.001

Note: \*\*\*represented significance at the 1% level.

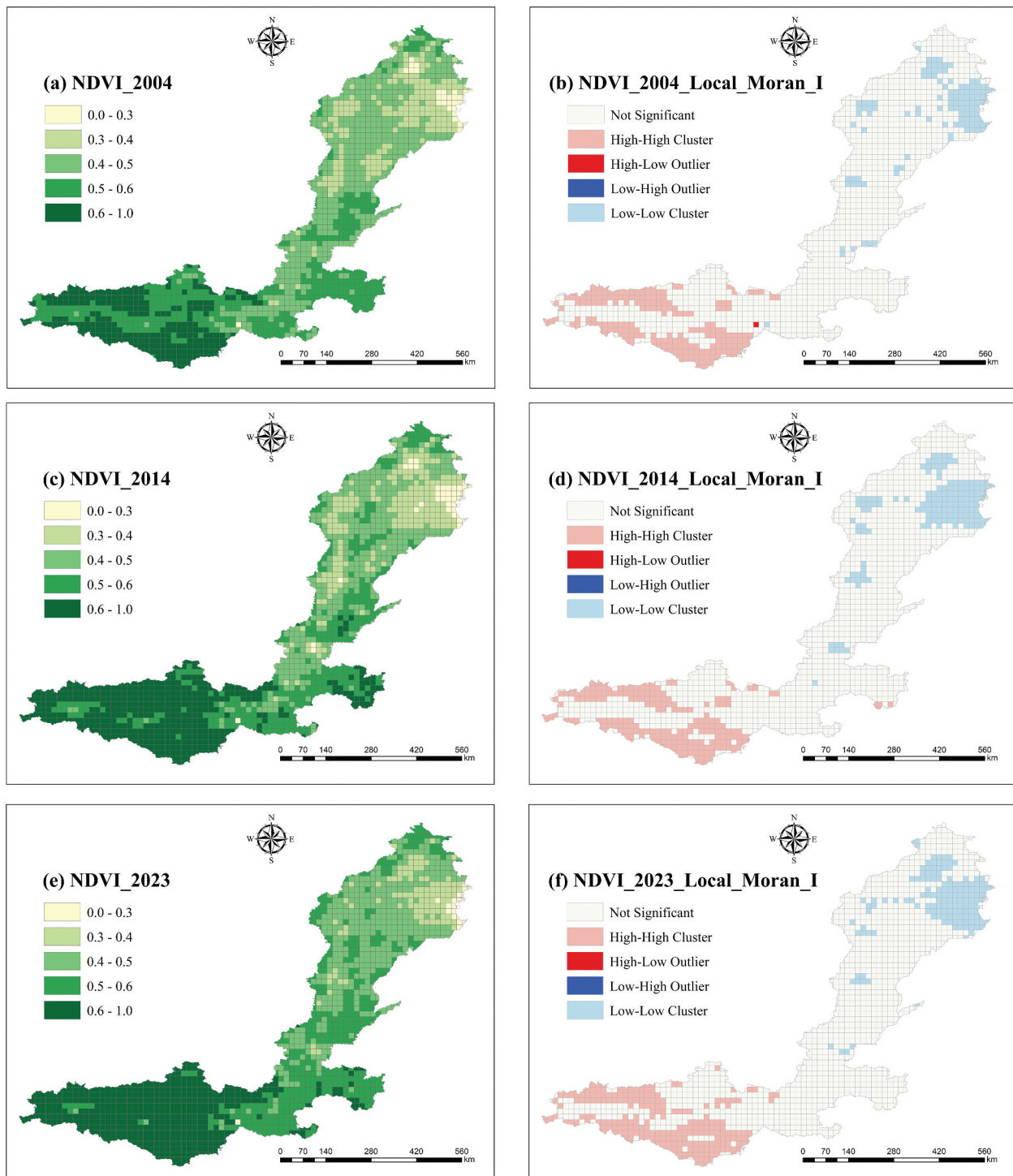


**Figure A1.** Spatial distribution of NDVI and corresponding local Moran's I cluster maps for the years 2004, 2014, and 2023. (a), (c), (e) showed NDVI values; (b), (d), (f) showed local Moran's I cluster types, including high-high, low-low, and spatial outliers.